DISSERTATION

Modeling of the Interaction of a Fluid Flow with a Thin Membrane as the Working Principle of a Double Channel Membrane Pump

ausgeführt zum Zwecke der Erlangung des akademischen Grades eines Doktors der technischen Wissenschaften unter der Leitung von

Ao.Univ.Prof. Dipl.-Ing. Mag.rer.nat. Dr.techn. Herbert Steinrück
E322
Institut für Strömungsmechanik und Wärmeübertragung

eingereicht an der Technischen UniversitätWien
Fakultät für Maschinenwesen und Betriebswissenschaften

von

Muhammad Asim
Matrikelnummer 0427364
1210 Wien, Donaufelderstrasse 54/2112

Wien, im April 2009

Abstract

A model to describe the working principle of a double channel membrane pump has been developed. The flow is driven by an interaction of an excited membrane with the surrounding fluid. Assuming high Reynolds number flow and small deflections of the membrane the linearized potential flow theory can be applied. Using the method of singularities an integral equation for the vorticity distribution along the membrane can be derived. It is supplemented with the Kutta condition for unsteady flows. Since the membrane is deformed by the pressure difference across the membrane the vorticity distribution and the shape of the membrane are determined simultaneously. A numerical method based on panel methods has been developed. The resulting equations are solved for a representative set of parameters and the overall performance parameters like the coefficient of efficiency and the net thrust of the pump are calculated. The results are discussed and the favorable parameter regimes are pointed out.

Zusammenfassung

Ein Modell zur Beschreibung der Arbeitsweise eine Doppelkanalmembranpumpe wurde entwickelt. Die Strömung wird durch eine Wechselwirkung einer angeregten Membran mit der umgebenden Flüssigkeit angetrieben. Unter Annahme einer Strömung mit hoher Reynolds-Zahl und kleinen Auslenkungen kann die Strömung als Potenzialströmung angesehen werden. Die Theorie der Umströmung zeitlich veränderlicher schlanker Profile kann für Umströmung der Membran in einem Kanal verallgemeinert werden. Um die Stärke der abgehenden Wirbel zu bestimmen, muss an der Hinterkante die Kuttabedingung für instationäre Strömungen erfüllt sein. Da die Membran durch die Druckdifferenz über der Membran verformt wird, müssen die Verteilung der Wirbelstärke und die Form der Membran gleichzeitig bestimmt werden. Eine numerische Methode, basierend auf Panelmethoden wird entwickelt. Die daraus resultierenden Gleichungen werden für einen representativen Satz von Parametern gelöst und der Wirkungsgrad sowie der Nettoschub der Pumpe werden berechnet. Die Ergebnisse werden diskutiert und die günstigen Parameterbereiche werden hervorgehoben.

Acknowledgment

I owe my profound thanks and deepest sense of gartitude to Almighty Allah, Creator of the universe, worthy of all praises, the merciful, who blessed me with determination, potential and ability to start this research work.

I would like to express my thanks to my parents, my wife, my sisters and my brothers, for their constant encouragement. Also to my friends for their help, support and constructive contributions.

Special thanks to the researchers at the Institute of Fluid Mechanics and Heat Transfer for their valuable input.

Finally, I would like to extend my gratitude to my supervisor, for his guidance, time and help during the course of this work.

Contents

List of Figures

List of Tables

List of Symbols

A	coefficient matrix at instant time t
a	dimensionless amplitude of flap motion
$\tilde{a}$	amplitude of flap motion
$\tilde{b}$	width of channel
F	dimensionless net thrust
$\tilde{F}$	net thrust
F_p	dimensionless horizontal component of pressure force
$\tilde{F}_p$	horizontal component of pressure force
F_{le}	dimensionless leading edge thrust
$\tilde{F}_{le}$	leading edge thrust
$\tilde{f}$	frequency of flap motion
h	dimensionless height of double channel
$\tilde{h}$	height of double channel
HW	coefficient matrix for induced velocity from wake
HIL	coefficient matrix for vorticity equation
i	index for vortices
j	index for panels
$\tilde{L}$	length of channel (reference length)
L_f	dimensionless length of flap
$\tilde{L}_f$	length of flap
L_m	dimensionless length of membrane
$\tilde{L}_m$	length of membrane
L_p	dimensionless length of rigid plate
$\tilde{L}_p$	length of rigid plate
N	number of panels
P_{in}	dimensionless power input
$\tilde{P}_{in}$	power input
P_m	dimensionless power input on the membrane
$\tilde{P}_m$	power input on the membrane

p	dimensionless pressure
$\tilde{p}$	pressure
t	dimensionless time
$\tilde{t}$	time
U	dimensionless velocity
$\tilde{U}$	velocity
$\tilde{U}_0$	dimensionless free stream velocity
$\tilde{U}_0$	free stream velocity
u	dimensionless velocity in x-direction
$\tilde{u}$	velocity in x-direction
v	dimensionless velocity in y-direction
$\tilde{v}$	velocity in y-direction
v_w	dimensionless velocity induced from wake
$\tilde{v}_w$	velocity induced from wake
w	dimensionless vertical position of membrane
$\tilde{w}$	vertical position of membrane
x	dimensionless horizontal coordinate
$\tilde{x}$	horizontal coordinate
$\tilde{x}_w$	horizontal coordinate in wake region
x_w	dimensionless horizontal coordinate in wake region
$\tilde{x}_0$	x-coordinate of leading edge of rigid plate
$\tilde{x}_f$	x-coordinate of leading edge of flap
$\tilde{x}_m$	x-coordinate of leading edge of membrane
x_{le}	dimensionless x-coordinate of leading edge
$\tilde{x}_{le}$	x- coordinate of leading edge
x_{te}	dimensionless x- coordinate of trailing edge
$\tilde{x}_{te}$	x- coordinate of trailing edge
y	dimensionless vertical coordinate
$\tilde{y}$	vertical coordinate

Greek Symbols

α	ratio of dynamic pressure to the lateral tension in the membrane
β	ratio of longitudinal tension to the lateral tension in the membrane
γ	dimensionless vorticity
γ_w	dimensionless vorticity in wake region
$\tilde{\gamma}$	vorticity
Γ	dimensionless circulation
Γ_w	dimensionless circulation in wake region
$\tilde{\Gamma}$	circulation
δ	length to height ratio of channel
Δp	dimensionless pressure difference
$\Delta\tilde{p}$	pressure difference
Δt	dimensionless time step
$\Delta\tilde{t}$	time step
Δx	dimensionless step size
Δx_w	dimensionless step size in wake region
$\Delta\tilde{x}$	step size
ϵ	dimensionless constant for input power on the membrane
$\tilde{\sigma}$	stress of membrane
$\tilde{\sigma}_x$	stress of membrane in x-direction
$\tilde{\sigma}_y$	stress of membrane in y-direction
$\tilde{\rho}$	density
η	propulsive efficiency of pump
ϕ	dimensionless complex potential
$\tilde{\phi}$	complex potential
ξ	dimensionless coordinate in x-direction
$\tilde{\xi}$	coordinate in x-direction
ψ	dimensionless coordinate in x-direction
$\tilde{\psi}$	coordinate in x-direction

Chapter 1

Introduction

1.1 Purpose of the Work

In this project the working principle of a new valveless pump 'the double channel membrane pump' will be investigated [77]. However, up to now most of the investigations on valveless pumping are concerned with physiology. Here a valveless pumping principle has been introduced which has the potential to be used in industrial applications. The design principal of the pump is shown in the Figure 1.1. A channel with rigid walls is divided in its mid plane into two sub-channels. On the inlet the sub-channels are separated by a rigid plate. At the trailing edge of the plate there is a flap which is moved periodically up and down. At the other end of the flap an elastic membrane is attached. Thus the motion of the flap will induce an excitation of the membrane. However, it is the interaction of the thin membrane with the surrounding fluid in both channels which drives a flow through the pump.

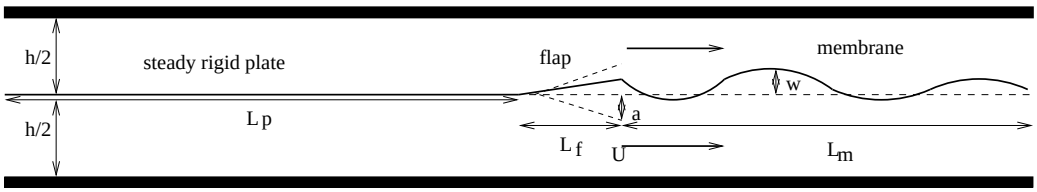

Figure 1.1: Sketch of double channel membrane pump

1.2 Literature Overview

This problem is considered as fluid structure interaction (FSI) problem. The coupling of thin membrane structure to the surrounding fluid flow is the main focus. Therfore a review on solid fluid interaction problems has been carried out. Valveless pumping in physiology is an active topic for researchers. Our model of double channel membrane pump is also a valveless pump and it can also be used for applications in industry. A review on valveless pumping has been carried out to grasp the valveless pumping effect. The motion of thin membrane is inspired from the propulsion of the slender fish and flights of small insects. We have reviewed here propulsion of animals. The flap used to excite the membrane resembles to the thin flapping foils. So an extensive review on the flapping foils have been done.

1.2.1 Fluid Solid Interactions

The numerical simulations of fluid solid interaction problems is a challenging task in scientific computations. Fluid solid interaction is used in coupled field analysis between fluid and solid structures. This phenomenon occurs when fluid flow deforms the solid structure and in return solid structure changes the fluid flow. Aeronautical engineering and Biomechanical engineering are two main fields where this phenomenon occurs. In aeronautical applications parachutes [61], airbags [45], sails [55], micro-air vehicles [35] are some examples of fluid solid interactions. In biomechanical engineering aortic valves [10, 11, 68], blood cells [56] can be given as examples of fluid structure interaction problems. There are many other areas where fluid structure interaction phenomenon is used like lightweight fabric building structures [20], automobile tires, underwaterexplosions etc.

1.2.2 Valveless Pumping

Gehart Liebau in 1954 first reported the valveless pumping effect. Liebau demonstrated a valveless pump comprised of an elastic tube that could pump fluid against a pressure gradient when periodically compressed from the ends. Thomann [63] presented a simple pumping mechanism in a valve less tube using assumptions like inviscid, one dimensional flow, long wavelength and small amplitude perturbations. E. Stemme and G. Stemme [58, 59] explored a valveless single chamber diffuser pump fabricated in brass using diffuser nozzle elements as flow rectifying elements. Olsson et Al. [48, 49] presented a planar double chamber pump fabricated in brass and then improved it fabricating in Ni. Jung and Peskin [28] described the two dimensional

numerical simulations of valveless pumping using the immersed boundary method. They demonstrated flow reversal dependent on forcing frequency. Their model was based on closed loop configuration and elastic restoring force. Ottsen [50] carried out one dimensional numerical simulations for a closed torus system with experimental validation. Borzi and Prospt [3] further investigated the Liebau phenomenon and proposed numerical models which showed that an open loop system could create a net pressure head. Rinderknecht et Al. [52] proposed a valveless, impedance-based micropump driven by electromagnetic actuation. An impedance pump is composed of an elastic section connected at the ends to rigid sections. In the valveless micro impedance pump reported by Wen [72], a lead zirconate titanate(PZT) actuator was used to deflect a thin film of Ni. The resulting resonance of the diaphragm vibration generated a larger diaphragm deflection, which consequently produced a greater driving pressure.

1.2.3 Propulsion of Animals

The flapping foil propulsion is inspired by the natural world. A large number of creatures such as birds , insects, fish use its wings, fin or tail for locomotion. We briefly review here the literature on propulsion of animals. Birds ability to generate thrust by means of flapping their wings first published by Knoller [31] and Betz [1]. The foremost known theory about propulsion of fish is the work of Lighthill. In an early work on this subject Lighthill [37] investigated swimming of fish that would generate high propulsive efficiency. In this study curvature of the fish was assumed small and the effect of vortex wake on fish was neglected. Later Lighthill [38] explored propulsive efficiencies in various aquatic locomotion modes using two dimensional slender body theory. Wu [73, 74] worked on hydrodynamics of swimming propulsion. Wu's theory examines fish propulsion as a two dimensional potential flow problem for a waving plate of finite chord and negligible thickness. The body profile is represented as a swimming plate with infinite degrees of freedom. Cheng et Al. [7] developed their vortex lattice panel method assuming infinitely thin fish and the undulations of small amplitude. Hill [57] developed a numerical boundary element method for large amplitude fish swimming for two and three-dimensional flow. Among others who studied propulsion of fish and other animals are Taylor [60], Gray [21, 22, 23], Webb [69, 70, 71], Daniel [8, 9], Huber [25], Drucker and Lauder [12, 13], Liu [41], Liu et Al. [39], Liu and Kawachi [40], Liu and Kato [42], Triantafyllou et Al. [64, 65, 66] etc.

1.2.4 Flapping Airfoils

In the beginning of the $20th$ century Knoller [31] and Betz [1] first described thrust production by an oscillating airfoil. They noted that vertical motion of an airfoil produces an effective angle of attack so that resulting normal force vector has a component in the forward direction. Katzmayr [30] in his experiment of wind tunnel measurements also observed this effect. Ober [47] provided additional theoretical explanations and simple calculations of Katzmayr's results. Birnbaum [2] first presented a solution for incompressible flow past flapping airfoils. Theodorsen [62] and Garrick [19] made theoretical calculations of an airfoil undergoing small amplitude heaving oscillations in an ideal fluid. Later Freymuth [18] experimentally demonstrated that an airfoil is capable of generating thrust when it undergoes either pure pitching or pure plunging. Thrust generation due to pitching was demonstrated by Koochesfahani [32]. A review on research and development of results of flapping wing propulsion was given by Rozhdestvensky and Ryzhov [53]. Lai and Platzer [33] and Jones et Al. [27] used a water tunnel to perform sinusoidally plunging oscillations of an airfoil. They compared the experimental data with their numerical computations by a incompressible potentail flow code. Using Euler equations Neef and Hummel [46] computed the two dimensional airfoils and three dimensional high aspect ratio wings. Lewin and Haj-Harari [34] modeled the thrust generation of a symmetric Joukowski heaving airfoil by solving vorticity equations for a two-dimensional incompressible viscous flow. Tuncer and Platzer [67] used compressible Navier-Stoke solver to compute the unsteady flow fields and obtained maximum propulsive efficiency when the flow remains mostly attached over the airfoil oscillated in combined pitching and plunging motion. Young and Lai [76] used a compressible Navier-Stoke solver and incompressible potential flow code to simulate the flow over sinusoidally plunging airfoil. Yang et Al. [75] computed the flow over an pitching and plunging airfoil using compressible Euler solver.

1.3 Thesis Organization

In the following chapters of this thesis, modeling approach, its numerical implimentation and results obtained are presented.

The second chapter deals with the modeling of the problem. It gives a detailed description of the flow model, linearized flow model, membrane model and the coupled membrane flow model. This is followed with dimensionless formulation of the problem. The wake convection has been discussed. At the

end of the chapter typical system parameters are also given.

The third chapter deals with numerical methods applied. A description of staggered grid is given. Steady and unsteady panel methods and there advantages and incapabilities are discussed in this chapter. The implimentation of the unsteady panel code is described in detail. Selection of number of panels used and number of wake points are discussed at the end of this chapter.

The fourth chapter deals with numerical results obtained for changing the parameters of the system.

The fifth chapter is the conclusion part which overviews the results obtained from different numerical simulations.

Chapter 2

Modeling

2.1 Potential Flow in a Channel

Consider a channel of length $\tilde{L}$ and height $\tilde{h}$. We suppose that the channel is infinitely extended at both ends along x-axis as shown in figure 2.1. The fluid flow enters the channel with free stream velocity $\tilde{U}_0$. There is a steady rigid plate of length $\tilde{L}_p$ at the beginning of the channel which divides the channel at its mid plane into two sub channels. The other end of the steady rigid plate is attached with flap of length $\tilde{L}_f$ which moves sinusoidally up and down along y-axis. At the rare end of the flap a thin membrane of length $\tilde{L}_m$ is attached. The flap excites the membrane and it starts moving. However the motion of the membrane is driven by the surrounding fluid flow. High Reynolds number flow is assumed. Also we suppose that flow is incompressible, irrotational and two dimensional. Therefore the flow can be represented by a potential function $\tilde{\phi}(\tilde{x}, \tilde{y})$ satisfying the Laplace equation.

$$\frac{\partial^2 \tilde{\phi}}{\partial \tilde{x}^2} + \frac{\partial^2 \tilde{\phi}}{\partial \tilde{y}^2} = 0. \tag{2.1}$$

Where

$$\frac{\partial \tilde{\phi}}{\partial \tilde{x}} = \tilde{u}, \tag{2.2}$$

$$\frac{\partial \tilde{\phi}}{\partial \tilde{y}} = \tilde{v}. \tag{2.3}$$

Here $\tilde{u}$ is longitudinal velocity component and $\tilde{v}$ is the vertical velocity component. The flow potential can be written as the super position of singular solutions of the Laplace equation. If we consider a single vortex of vorticity strength $\tilde{\Gamma}$ at the center of the channel ($\tilde{y} = 0$) the flow potential

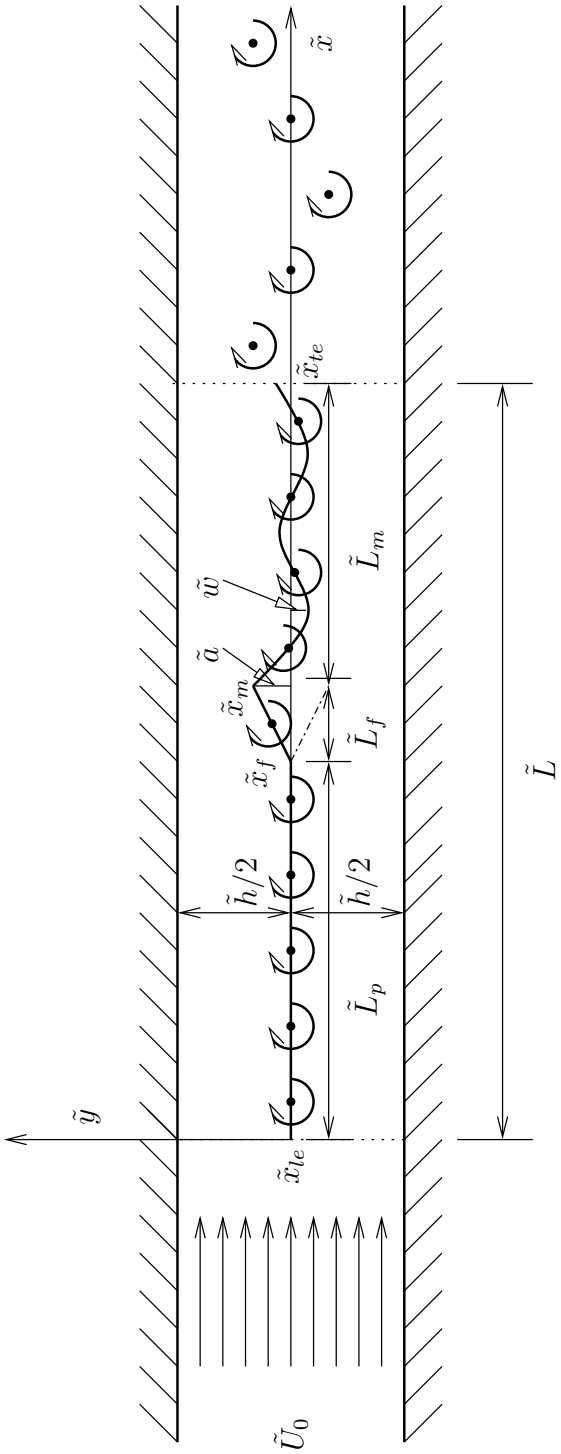

Figure 2.1: Problem formulation

for a this single vortex in the middle of the channel can be found in Katz [29] and it is given as

$$\tilde{\phi}(\tilde{z}) = \frac{-i\tilde{\Gamma}}{2\pi} \ln[\tanh \frac{\pi \tilde{z}}{2\tilde{h}}]. \tag{2.4}$$

Now if we consider many vortices on the steady rigid plate, flap, membrane and in the wake as shown in figure 2.1. The complex potential for all these vortices would be given as [29, 54]

$$\tilde{\phi}(\tilde{z}, \tilde{t}) = \tilde{U}_0 \tilde{z} - \frac{i}{2\pi} \int_{\tilde{x}_{le}}^{\infty} \tilde{\gamma}(\tilde{\xi}) \ln[\tanh \frac{\pi(\tilde{z} - \tilde{\xi})}{2\tilde{h}}] d\tilde{\xi}, \tag{2.5}$$

or

$$\begin{aligned} \tilde{\phi}(\tilde{z}, \tilde{t}) = \tilde{U}_0 \tilde{z} &- \frac{i}{2\pi} \int_{\tilde{x}_{le}}^{\tilde{x}_{te}} \tilde{\gamma}(\tilde{\xi}) \ln[\tanh \frac{\pi(\tilde{z} - \tilde{\xi})}{2\tilde{h}}] d\tilde{\xi} \\ &- \frac{i}{2\pi} \int_{\tilde{x}_{te}}^{\infty} \tilde{\gamma}_w(\tilde{\xi}) \ln[\tanh \frac{\pi(\tilde{z} - \tilde{\xi})}{2\tilde{h}}] d\tilde{\xi}. \end{aligned} \tag{2.6}$$

By partial integration we obtain

$$\begin{aligned} \tilde{\phi}(\tilde{z}, \tilde{t}) = \tilde{U}_0 \tilde{z} &- \frac{i}{2\pi} \Gamma(\tilde{x}_{te}) \ln \tanh \frac{\pi(\tilde{z} - \tilde{x}_{te})}{2\tilde{h}} \\ &+ \frac{i}{2\pi} \tilde{\Gamma}(\tilde{x}_{le}) \ln \tanh \frac{\pi(\tilde{z} - \tilde{x}_{le})}{2\tilde{h}} \\ - \frac{i}{2\tilde{h}} \int_{\tilde{x}_{le}}^{\tilde{x}_{te}} &\frac{\Gamma(\xi) d\xi}{\sinh \frac{\pi(\tilde{x} - \tilde{\xi})}{\tilde{h}}} - \frac{i}{2\tilde{h}} \int_{\tilde{x}_{te}}^{\infty} \frac{\gamma_w(\xi) d\xi}{\sinh \frac{\pi(\tilde{x} - \tilde{\xi})}{\tilde{h}}}, \end{aligned} \tag{2.7}$$

where

$$\tilde{\Gamma} = \int_{\tilde{x}_{le}}^{\tilde{x}_{te}} \tilde{\gamma}(\tilde{\xi}) d\tilde{\xi}. \tag{2.8}$$

If the logarithms are defined $0 \leq \arg \tilde{z} \leq 2\pi$ then the complex velocity is given by

$$\tilde{u} - i\tilde{v} = \tilde{U}_0 - \frac{i}{2\tilde{h}} \int_{\tilde{x}_{le}}^{\infty} \tilde{\gamma}(\tilde{\xi}) \frac{d\tilde{\xi}}{\sinh \frac{\pi(\tilde{z} - \tilde{\xi})}{\tilde{h}}}. \tag{2.9}$$

2.1.1 Linearized Flow Model

Now consider the vortices are distributed only along the center line of the channel as shown in figure 2.2. The potential at the center line considering the small perturbation flow is given by

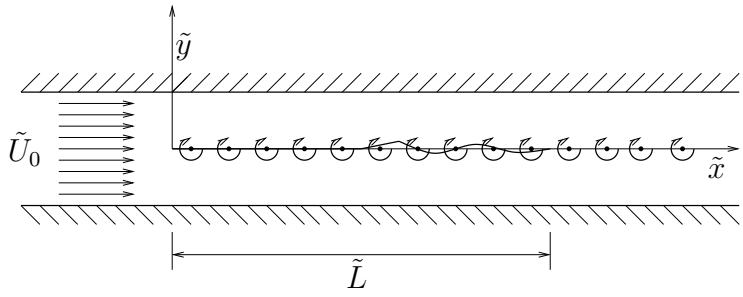

Figure 2.2: Linearized problem

$$\tilde{\phi}(\tilde{x},\pm 0) = \tilde{U}_0\tilde{x} - (\pm\frac{1}{2})(\tilde{\Gamma}(\tilde{x},\tilde{t}) - \tilde{\Gamma}(\tilde{x}_{le},\tilde{t})) + \frac{1}{2}(\tilde{\Gamma}(\tilde{x}_{te},\tilde{t}) - \tilde{\Gamma}(\tilde{x}_{le},\tilde{t})). \tag{2.10}$$

The velocities of the center line using small perturbation potential are

$$\tilde{u}(\tilde{x},\pm 0) = \tilde{U}_0 - (\pm\frac{\tilde{\gamma}(\tilde{x})}{2}), \tag{2.11}$$

$$\tilde{v}(\tilde{x},0) = \frac{1}{2\tilde{h}}\int_{\tilde{x}_{le}}^{\infty}\tilde{\gamma}(\tilde{\xi})\frac{d\tilde{\xi}}{\sinh\frac{\pi(\tilde{x}-\tilde{\xi})}{\tilde{h}}}. \tag{2.12}$$

At the leading edge we can have

$$\tilde{\Gamma}(\tilde{x}_{le},\tilde{t}) = 0.$$

Thus pressure difference across the vortex sheet is

$$\Delta\tilde{p} = \tilde{p}(\tilde{x},0+) - \tilde{p}(\tilde{x},0-). \tag{2.13}$$

From the Bernouli's equation the pressure difference would be

$$\Delta\tilde{p} = -\tilde{\rho}[\tilde{\phi}_{\tilde{t}}(\tilde{x},0+) - \tilde{\phi}_{\tilde{t}}(\tilde{x},0-) + \frac{1}{2}\{\tilde{\phi}_{\tilde{x}}^2(\tilde{x},0+) + \tilde{\phi}_{\tilde{y}}^2(\tilde{x},0+) - \tilde{\phi}_{\tilde{x}}^2(\tilde{x},0-) - \tilde{\phi}_{\tilde{y}}^2(\tilde{x},0-)\}]. \tag{2.14}$$

So the linearized form of pressure difference is given as

$$\Delta\tilde{p} = \tilde{\rho}(\tilde{\Gamma}_{\tilde{t}}(\tilde{x},\tilde{t}) + \tilde{U}_0\tilde{\gamma}(\tilde{x},\tilde{t})). \tag{2.15}$$

2.1.2 Kinematic Boundary Condition

When we have an impermeable boundary the fluid flow relative to the boundary must be tangential to it. If the fluid boundary is fixed type in space, the fluid velocity component normal to the boundary must be zero and if the boundary is moving type then the normal component of the fluid must be equal to the velocity of the boundary normal to itself. In other words the solid body surface does not allow the flow through it. This means that difference of the fluid velocity and the body surface velocity in the direction normal to the body surface should be zero. Thus the kinematic boundary condition is given as

$$\tilde{v}(\tilde{x},\tilde{w}(\tilde{x},\tilde{t}),\tilde{t}) = \tilde{u}(\tilde{x},\tilde{w}(\tilde{x},\tilde{t}),\tilde{t})\tilde{w}_{\tilde{x}}(\tilde{x},\tilde{t}) + \tilde{w}_{\tilde{t}}(\tilde{x},\tilde{t}). \tag{2.16}$$

We consider here the case of a small amplitude. Therefore

$$\tilde{v}(\tilde{x},0,\tilde{t}) = \tilde{U}_0\tilde{w}_{\tilde{x}}(\tilde{x},\tilde{t}) + \tilde{w}_{\tilde{t}}(\tilde{x},\tilde{t}). \tag{2.17}$$

Using (2.12) we get the following vorticity equation

$$\frac{1}{2\tilde{h}}\int_{\tilde{x}_{le}}^{\infty}\tilde{\gamma}(\tilde{\xi})\frac{d\tilde{\xi}}{\sinh\frac{\pi(\tilde{x}-\tilde{\xi})}{\tilde{h}}} = \tilde{U}_0\tilde{w}_{\tilde{x}}(\tilde{x},\tilde{t}) + \tilde{w}_{\tilde{t}}(\tilde{x},\tilde{t}). \tag{2.18}$$

Expanding for the wake region the above equation can be written as

$$\begin{aligned}\frac{1}{2\tilde{h}}\int_{\tilde{x}_{le}}^{\tilde{x}_{te}}\tilde{\gamma}(\tilde{\xi})\frac{d\tilde{\xi}}{\sinh\frac{\pi(\tilde{x}-\tilde{\xi})}{\tilde{h}}} - \tilde{U}_0\tilde{w}_{\tilde{x}}(\tilde{x},\tilde{t}) - \tilde{w}_{\tilde{t}}(\tilde{x},\tilde{t})& \\ = -\frac{1}{2\tilde{h}}\int_{\tilde{x}_{le}}^{\infty}\tilde{\gamma}_w(\tilde{\xi})\frac{d\tilde{\xi}}{\sinh\frac{\pi(\tilde{x}-\tilde{\xi})}{\tilde{h}}}.&\end{aligned} \tag{2.19}$$

Where $\tilde{\gamma}_w(\tilde{\xi})$ is the vorticity strength of the vortices in the wake region.

2.1.3 Kutta Condition

The Kutta condition at the trailing edge for unsteady flows is given in Katz [29]. It can be mathematically written as

$$\tilde{\gamma}_w(\tilde{x}_{te},\tilde{t}) = -\frac{1}{\tilde{U}_0}\tilde{\Gamma}_{\tilde{t}}(\tilde{x}_{te},\tilde{t}). \tag{2.20}$$

2.1.4 Wake

Since $\tilde{\Gamma}$ is not constant vortices are shed into the wake at the trailing edge of the membrane. We have to link the body to its wake and have to solve the system for unknown wake vortices strength. The total circulation of the body and vorticity of the wake must be equal at each time step according to the Kelvin's circulation theorem [29]. This means the vorticity lost by the body is equal to the strength of new vortex shed at each time step. This can be mathematically represented as

$$\tilde{\gamma}_{w,\tilde{t}} + \tilde{U}_0 \gamma_{w,\tilde{x}} = 0, \tag{2.21}$$

$$\tilde{\gamma}_w(\tilde{x}_{te}, \tilde{t}) = \tilde{\gamma}(\tilde{x}_{te}, \tilde{t}). \tag{2.22}$$

2.2 Membrane Model

A structure whose thickness is small when compared to the surface dimensions and has negligible bending rigidity is called membrane. A membrane can be considered two dimensional analogy of a string. Here we consider a rectangular thin membrane undergoing small deformations under the external forces. The thickness of the membrane and its properties are assumed to be uniform. One end of the membrane is attached with the flap while other edge is free to move. In our model two external forces are acting on the membrane, the pressure force from the fluid flow and the actuator force from flap. The flap has a prescribed motion. For a simple model we have following assumptions for the membrane

- Mass of the membrane is negligible.
- Small deformations $\tilde{w}(\tilde{x}, \tilde{t})$ of the membrane.
- The membrane is thin and the bending stiffness can be neglected.
- The strains in the membrane are small.
- No wrinkling of the membrane occurs.
- The material of the membrane is isotropic.

Denoting the pressure difference across the membrane by $\Delta\tilde{p}$ we have from the mechanics of the solid bodies [51]

$$\Delta\tilde{p} = \tilde{\sigma}\Delta\tilde{w}. \tag{2.23}$$

Where $\tilde{\sigma}$ is the stress of the membrane in non excited state. The stress has two components the longitudinal component $\tilde{\sigma}_x$ and the vertical component $\tilde{\sigma}_y$.

2.3 Coupled Membrane Equation

The linearized flow model can be coupled to the membrane equation. Using equation (2.15) and equation (2.23) we get the coupled membrane equation

$$\tilde{\sigma}\nabla\tilde{w} = \tilde{\rho}(\tilde{\Gamma}_{\tilde{t}}(\tilde{x},\tilde{t}) + \tilde{U}_0\tilde{\gamma}(\tilde{x},\tilde{t})) \quad : \quad \tilde{x}_m \leq \tilde{x} \leq \tilde{x}_{te}, \tag{2.24}$$

where $\tilde{x}_m$ is the leading edge of the membrane and $\tilde{x}_{te}$ is the trailing edge of the membrane.

2.3.1 Motion of Flap

There is a steady rigid plate at the beginning of the channel as shown in figure 2.1. At the trailing edge of steady rigid plate a flap is attached which moves sinusoidally up and down. Flap excites the membrane motion. The motion of the flap is given by

$$\tilde{w}(\tilde{x}_m,\tilde{t}) = \tilde{a}\sin(2\pi\tilde{f}\tilde{t}). \tag{2.25}$$

2.4 Thrust of the Pump

The horizontal force acting on the body surface in negative x-direction is called net thrust of the pump. The net thrust on thin swimming bodies can be found in Wu [73]. The net thrust of the pump is given as

$$\tilde{F} = \tilde{F}_p + \tilde{F}_{le}. \tag{2.26}$$

Where $\tilde{F}_p$ is the horizontal component of the pressure force and $\tilde{F}_{le}$ is the leading edge thrust.

2.4.1 Horizontal Pressure Force

The periodic horizontal pressure force on the body is given as [73]

$$\tilde{F}_p = \frac{1}{\tilde{T}}\int_0^{\tilde{T}}\int_{\tilde{x}_{le}}^{\tilde{x}_{te}} \tilde{w}_{\tilde{x}}\Delta\tilde{p}d\tilde{x}d\tilde{t}. \tag{2.27}$$

Where $\Delta\tilde{p}$ is the pressure difference across the membrane, $\tilde{w}_{\tilde{x}}$ is the slope of the vertical position and $\tilde{T}$ is the time period.

2.4.2 Leading Edge Thrust

The leading edge thrust results from the singularity of the vortex at the leading edge. The leading edge thrust can be approximated using Blasius formula as discussed by Wu [73]. The leading edge thrust is given as

$$\tilde{F}_{le} = -\frac{\pi}{4}\rho\tilde{K}_{\tilde{\gamma}}(\tilde{t})^2. \tag{2.28}$$

The value of the $\tilde{K}_{\tilde{\gamma}}(\tilde{t})$ can be approximated as

$$\tilde{K}_{\tilde{\gamma}}(\tilde{t}) = \lim_{\tilde{x}\to 0} \tilde{\gamma}(\tilde{x})\sqrt{\tilde{x}}. \tag{2.29}$$

2.5 Input Power

If the prescribed motion has to be maintained there must be an external force which is opposite to the pressure force on the membrane. The periodic input power as discussed in [73] is given as

$$\tilde{P}_{in} = \frac{1}{\tilde{T}}\int_0^{\tilde{T}}\int_{\tilde{x}_{le}}^{\tilde{x}_{te}} \tilde{w}_{\tilde{t}}\Delta p d\tilde{x}d\tilde{t}. \tag{2.30}$$

Here $\tilde{w}_{\tilde{t}}$ is the time derivative of vertical position, $\Delta\tilde{p}$ is the pressure difference across the body and $\tilde{T}$ is time period.

2.5.1 Input Power on the Membrane

The input power on the membrane can be found from equation (2.30). The power input on the membrane would be

$$\tilde{P}_{m} = \frac{1}{\tilde{T}}\int_0^{\tilde{T}}\int_{\tilde{x}_{m}}^{\tilde{x}_{te}} \tilde{w}_{\tilde{t}}\Delta p d\tilde{x}d\tilde{t}. \tag{2.31}$$

Using equation (2.23) for pressure difference across the membrane we have

$$\tilde{P}_{m} = \frac{1}{\tilde{T}}\int_0^{\tilde{T}}\int_{\tilde{x}_{m}}^{\tilde{x}_{te}} \tilde{\sigma}\tilde{w}_{\tilde{t}}\Delta\tilde{w} d\tilde{x}d\tilde{t}. \tag{2.32}$$

Integrating this equation over the length of membrane we can find the input power on the membrane which is given as

$$\tilde{P}_{m} = \frac{1}{\tilde{T}}\int_0^{\tilde{T}} \tilde{\sigma}_{\tilde{x}}\tilde{w}_{\tilde{t}}\tilde{w}_{\tilde{x}} d\tilde{t}. \tag{2.33}$$

Table 2.1: Parameters describing double channel membrane pump

$\tilde{L}$	reference Length
$\tilde{L}_f$	length of flap
$\tilde{L}_p$	length of plate
$\tilde{L}_m$	length of membrane
$\tilde{h}$	height of double channel
$\tilde{b}$	width of channel
$\tilde{a}$	amplitude of flap motion
$\tilde{f}$	frequency of flap motion
$\tilde{u}$	velocity in horizontal direction
$\tilde{v}$	velocity in vertical direction
$\tilde{U_0}$	free stream velocity
$\tilde{\sigma}_x$	longitudinal tension in the membrane
$\tilde{\sigma}_y$	lateral tension in the membrane

2.6 Propulsive Efficiency of the Pump

The efficiency of the propulsion of the pump would be [73]

$$\eta = \frac{\tilde{F}\tilde{U}_\infty}{\tilde{P}_{in}}. \tag{2.34}$$

Here $\tilde{U}_\infty$ is the free stream velocity, $\tilde{F}$ is the net thrust of the pump and $\tilde{P}_{in}$ is the power required to maintain the motion.

2.7 Dimensionless Formulation

The first step to analyze the flow will be a dimensional analysis. We scale for all related quantities with appropriate reference values and then form dimensionless parameters. There are many advantages of dimensional analysis. For example the number of parameters in the problem are reduced and it allows the comparison of flow configuration of different sizes. Most important parameters describing the double channel membrane pump are given in table 2.1. The total length of channel (see figure 2.1) is taken as reference length in the horizontal direction and all the other lengths in horizontal direction

are scaled with this length

$$\tilde{L}_p = L_p \tilde{L}, \tag{2.35}$$
$$\tilde{L}_f = L_f \tilde{L}, \tag{2.36}$$
$$\tilde{L}_m = L_m \tilde{L}. \tag{2.37}$$

The vertical position of the membrane $\tilde{w}$ is scaled with the amplitude of the flap $\tilde{a}$

$$\tilde{w} = \tilde{a} w. \tag{2.38}$$

Time is scaled with the frequency of the motion of the flap

$$\tilde{t} = \frac{1}{\tilde{f}} t. \tag{2.39}$$

The longitudinal velocity $\tilde{u}$ and the vertical velocity $\tilde{v}$ are scaled accordingly.

$$\tilde{u} = \tilde{U}_0 + \tilde{a}\tilde{f} u, \tag{2.40}$$
$$\tilde{v} = \tilde{a}\tilde{f} v. \tag{2.41}$$

Here $\tilde{U}_0$ is free stream velocity and $\tilde{f}$ is the frequency of the motion of the flap. The vorticity $\tilde{\gamma}$ and total circulation $\tilde{\Gamma}$ are scaled accordingly.

$$\tilde{\gamma} = \tilde{f}\tilde{a}\gamma, \tag{2.42}$$
$$\tilde{\Gamma} = \tilde{f}\tilde{a}\tilde{L}\Gamma. \tag{2.43}$$

As we have prescribed motion of the flap therefore pressure difference across the membrane $\Delta\tilde{p}$ is scaled with pressure due to velocity of the fluctuation instead of the stagnation pressure. The force on the membrane and input power are scaled accordingly.

$$\Delta\tilde{p} = \tilde{\rho}\tilde{f}^2\tilde{a}\tilde{L}\Delta p, \tag{2.44}$$
$$\tilde{F} = \tilde{\rho}\tilde{f}^2\tilde{a}^2\tilde{L}\tilde{F}, \tag{2.45}$$
$$\tilde{P}_{in} = \tilde{\rho}\tilde{f}^3\tilde{a}^2\tilde{L}^2\tilde{P}_{in}. \tag{2.46}$$

2.7.1 Coupled Membrane Equation

The membrane equation (2.24) in dimensionless form will be

$$\beta w_{xx} - w = \alpha[\Gamma_t(x,t) + \frac{1}{Sr}\gamma(x,t)]. \tag{2.47}$$

Where

$$\alpha = \frac{\tilde{\rho}\tilde{f}^2\tilde{L}\tilde{b}^2}{2\tilde{\sigma}_{\tilde{y}}}, \tag{2.48}$$

$$\beta = \frac{\tilde{\sigma}_{\tilde{x}}\tilde{b}^2}{2\tilde{\sigma}_{\tilde{y}}\tilde{L}^2}, \tag{2.49}$$

$$Sr = \frac{\tilde{f}\tilde{L}}{\tilde{U}_0}. \tag{2.50}$$

Here α, β, Sr are dimensionless numbers. The α is the ratio of dynamic pressure to the lateral tension in the membrane. The β is the ratio of the longitudinal tension to the lateral tension in the membrane where as Sr is the Strouhal number which is the ratio of the fluctuation velocity to the free stream velocity. Therefore dimensionless membrane equation can be written as

$$\beta w_{xx} - w - \alpha[\int_0^x \gamma_t(\xi, t) + \frac{1}{Sr}\gamma(x, t)] = 0. \tag{2.51}$$

2.7.2 Motion of Flap

The dimensionless motion of the flap have been computed by applying scaling on the equation (2.25)

$$w(x_m, t) = \sin(2\pi t). \tag{2.52}$$

2.7.3 Vorticity Equation

The vorticity equation (2.19) in dimensionless form will be

$$\begin{aligned} \frac{\delta}{2}\int_0^1 \gamma(\xi)\frac{d\xi}{\sinh \pi\delta(x-\xi)} - \frac{1}{Sr}w_x - w_t \\ = -\frac{\delta}{2}\int_1^\infty \gamma_w(\xi)\frac{d\xi}{\sinh \pi\delta(x-\xi)} \end{aligned} \tag{2.53}$$

Where

$$\delta = \frac{\tilde{L}}{\tilde{h}}, \tag{2.54}$$

$$Sr = \frac{\tilde{f}\tilde{L}}{\tilde{U}_0}. \tag{2.55}$$

Sr is the Strouhal number as explained earlier whereas δ is the aspect ratio of the pump.

2.7.4 Wake

The dimensionless form of the wake has been obtained by applying the scaling laws on equation (2.21)

$$\gamma_{w,t} + \frac{1}{Sr}\gamma_{w,x} = 0, \tag{2.56}$$

$$\gamma_w(1,t) = \gamma(1,t). \tag{2.57}$$

2.7.5 Kutta Condition

The dimensionless form of the unsteady Kutta condition has been established by applying the scaling on equation (2.20)

$$\int_0^1 \gamma_t dx + \frac{1}{Sr}\gamma(1,t) = 0. \tag{2.58}$$

2.7.6 Wake Convection

The vortices which are shed into the wake have effect on the motion of the membrane. To calculate velocity induced from the wake we have to cut the wake at some point. For periodic solutions we describe the wake using period length. The length of a period is given as $1/Sr$. Therefore

$$\gamma_w(x + \frac{1}{Sr}) = \gamma_w(x). \tag{2.59}$$

The velocity induced from the wake can be approximated by assuming the periodic state.

$$v_w(x) = \frac{\delta}{2}\int_1^\infty \gamma_w(\xi)\frac{d\xi}{\sinh \pi\delta(x-\xi)}, \tag{2.60}$$

$$= \frac{\delta}{2}\sum_{k=0}^{\infty}\int_{1+k/Sr}^{1+(k+1)/Sr} \gamma_w(\xi)\frac{d\xi}{\sinh \pi\delta(x-\xi)}, \tag{2.61}$$

$$= \int_{1/Sr}^{0} \gamma_w(1+\psi)\sum_{k=0}^{\infty}\frac{\delta}{2}\frac{d\psi}{\sinh \pi\delta(x-1-\psi-k/Sr)}. \tag{2.62}$$

Where, $\xi = k/Sr + 1 + \psi$

2.7.7 Performance Parameters

The performance parameters of the pump are non dimensionalized by applying scaling laws on respective equations. The non dimensional horizontal

pressure force can be obtained by applying scaling laws on equation (2.27) and it is given as

$$F_p = \int_0^1 \int_0^1 w_x \Delta p dx dt. \tag{2.63}$$

Using equation (2.28) leading edge thrust in dimensionless form would be

$$F_{le} = -\frac{\pi}{4} K_\gamma(t)^2. \tag{2.64}$$

Where the value of $K_\gamma(t)$ is given as

$$K_\gamma(t) = \lim_{x \to 0} \gamma(x) \sqrt{x}. \tag{2.65}$$

The dimensionless input power is obtained by applying scaling laws on equation (2.30)

$$P_{in} = \int_0^1 \int_0^1 w_t \Delta p dx dt. \tag{2.66}$$

The input power for membrane in dimensionless form can be calculated using equation (2.33)

$$P_m = \int_0^1 \epsilon w_t w_x dt. \tag{2.67}$$

Where ϵ is dimensionless constant and its value is given by

$$\epsilon = \frac{\tilde{\sigma}_{\tilde{x}}}{\tilde{\rho} \tilde{f}_2 \tilde{L}^3}. \tag{2.68}$$

The propulsive efficiency of the pump in dimensionless form can be obtained by applying scaling laws on equation (2.34).

$$\eta = \frac{F}{P_{in} Sr} \tag{2.69}$$

Here Sr is the Strouhal number as explained earlier, F is the dimensionless net thrust of the pump and P_{in} is the dimensionless power input.

2.8 Typical System parameters

The following parameters for the fluid and the thin membrane have been used for all the simulations performed under the present study.

2.8.1 Dimensional Parameters

The structural values were obtained from [77]. These values are shown in table 2.2.

Table 2.2: Typical dimensional parameters

Parameter	**Symbol**	**Value**	**Units**
Longitudinal tension	$\tilde{\sigma}_x$	3.12	N/mm
Lateral tension	$\tilde{\sigma}_y$	1.62	N/mm
Fluid density	$\tilde{\rho}$	998.2	Kg/m^3
Frequency of flap	$\tilde{f}$	20.0	Sec^{-1}
Thickness of membrane	$\tilde{b}$	10.0	cm

Table 2.3: Typical dimensionless constants

Parameter	**Symbol**	**Value**
Tension in the membrane	α	1.23234
Tension in the membrane	β	0.00963
Strouhal number	Sr	10.0
Aspect ratio	δ	10.0

2.8.2 Dimensionless Parameters

The dimensionless constants used here, tensions in the membrane α and β, length to width ratio of the channel δ and Strouhal number Sr control the whole simulation. In table 2.3 typical values for these constants are given.

Chapter 3

Numerical Methods

In this chapter all methods to implement numerically the modeling approach discussed in chapter 2 will be discussed. At first the discretization methods and then implementation of panel methods and finite difference methods will be presented.

3.1 Staggered Grid

In our problem we have to calculate two variables the vorticity $\gamma(x,t)$ and the vertical position $w(x,t)$ of the membrane. The straightforward approach to calculate these variables is to use an unstaggered grid or uniform grid. On a staggered grid the physical variables are located at different positions. In our case the vorticity $\gamma(x,t)$ has been calculated at center of each panel $(x_{i-\frac{1}{2}})$. Where as the vertical position $w(x,t)$ has been calculated at end points of each panel (x_i). In figure 3.1 a staggered grid with variables location is shown.

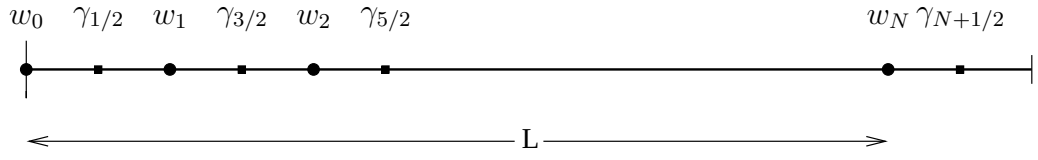

Figure 3.1: Staggered grid

3.2 Panel Methods

Many authors have discussed the theory of panel methods. Hess and Smith described these methods in detail [6, 29]. Since panel methods are the core of this investigation it is necessary to lay some ground work for panel methods. The simplest CFD methods are linear solvers. Panel methods are used to solve linear differential equations such as the Prandtl-Glauert equation and the Laplace equation. Panel methods are based on idea that sources or vortices of some strength are located in the flow such that their combined solutions satisfy the boundary conditions of the problem. The boundary conditions are typically that the surface is impermeable (flow does not go through the surface) and the flow approaches the freestream solution far from the body.

3.2.1 Advantages of Panel Methods

Panel methods have been the workhorse of the aircraft industry. They have been used, almost exclusively, to analyze the forces on the aircraft [29]. The main advantages of panel methods are

- They can calculate the gas or liquid flow around the complex configurations such as aircraft with relative ease.
- Panel methods are faster when compared to the finite difference methods that compute the flow properties in the entire field.
- Panel methods are also capable of accommodating flexibility and interference effects which makes them more useful when analyzing the aerodynamic forces on flapping wings.
- They take account of the linearity of the Laplace equation and avoid the requirement to generate a grid needed in finite difference and finite volume methods for obtaining inviscid flow solutions.
- They are the best when modeling fully attached, high Reynolds number, subsonic flow.

3.2.2 Incapabilities of Panel Methods

Along with many advantages there are some incapabilities of panel methods.

- Panel methods are incapable of modeling the viscous effects that are evident in all real flows.

- They are unable to predict boundary layer and flow separation.
- Panel methods can not model rotational flows.
- They can not model supersonic flows.

3.3 Steady State Panel Method

Panel methods can be divided into steady state panel methods and unsteady panel methods. Although real interest in this work is about unsteady panel method, basics of steady model also have been discussed. The main steps for steady state model are

- Selection of singularity elements
- Discretization of the geometry and grid generation
- Computation of influence coefficients
- Enforcement of Kutta condition
- Solving the set of linear equations
- Computation of the horizontal forces

3.3.1 Selection of Singularity Elements

First of all the selection of singularity elements have been made. Singularity elements can be sources or sinks and vortices of different types. We have chosen discrete point vortices.

3.3.2 Discretization of the Geometry and Grid Generation

The total length has been divided into N panels. The length of the panels can be variable or constant. In our case we have kept the length of the panels constant. At the center of each panel a discrete vortex element has been placed. The kinematic boundary condition will be enforced at the end point of each panel.

3.3.3 Computation of Influence Coefficients

As discussed before the flow around the solid boundary satisfies the Laplace's equation

$$\nabla^2\phi = 0. \tag{3.1}$$

The singularity elements (vortices) placed on the surface of the body induce velocities. The total velocity at any point can be computed as the sum of free stream velocity and the velocity induced by these singularities.

$$U = U_\infty + u. \tag{3.2}$$

We apply Neuman's boundary condition at the solid boundary. These boundary conditions require the velocity normal to the surface of the body to be zero.

$$(U_\infty + u).n = 0. \tag{3.3}$$

Here n is the normal vector to the surface of the body. Since U_∞ is the known free stream velocity. Therefore it can be moved to the right hand side.

$$u.n = -U_\infty.n. \tag{3.4}$$

Then the induced velocities by each vortex at respective control point are calculated. Now the left hand side can be written as

$$u.n = \sum_{j=1}^{N} a_{ij}\Gamma_j. \tag{3.5}$$

This is self induced part. The influence of each vortex at each control point has to be computed. So the influence coefficients a_{ij} represent the velocity component normal to the surface of the body for a unit strength vortex element Γ_j at control point i

$$a_{ij} = (u, v)_{1j}.n1. \tag{3.6}$$

Therefor the boundary condition at control point 1 can be expressed as

$$a_{11}\Gamma_1 + a_{12}\Gamma_2 + \ldots + a_{1N}\Gamma_N + U_\infty.n_1 = 0. \tag{3.7}$$

Where Γ_j is the unknown circulation. In this way applying the boundary condition on all the control points we can build matrix of influence coefficients.

3.3.4 Solving the Set of Linear Equations

After calculating the influence coefficients at each control point and applying the Kutta condition and the boundary condition for all the panels and known right hand side a set of linear equations is established.

$$\sum_{j=1}^{N} a_{ij}\Gamma_j = RHS_i. \tag{3.8}$$

Here the circulations Γ_j are the strengths of singularities which we have to compute. This system of equations can be solved using any standard linear equation solver.

3.3.5 Computation of the Horizontal Forces

After computing the circulation for every panel we can calculate the horizontal forces. Applying Bernouli's equation we can calculate the pressure distribution on the surface of the body. All the other forces then can be calculated from this pressure distribution.

3.4 Unsteady Panel Method

An unsteady panel method code was developed following Hess and Smith [6, 29]. At low speeds and low frequency we may approximate the unsteady effects of our oscillating membrane with continuous distribution of vorticity along the center line. The vorticity can be approximated by discrete vortices. As the membrane moves it leaves a vortex wake at the trailing edge. The inviscid incompressible flow solver uses N constant strength discrete vortex panels to represent the plate, actuator and membrane. Each vortex panel is assumed to have same strength. A zero normal velocity constraint is applied at the center of each panel. This ensures that flow past the plate, actuator and membrane is tangential. The Kutta condition is applied at the trailing edge. The total vorticity of the vortex panels is determined by the application of the Kutta condition. The vorticity shed into the wake as a result of membrane motion is modeled in the unsteady panel code as a series of discrete point vortices. These vortices are convected at each time step. Calculation of pressure difference in unsteady potential flows requires use of unsteady Bernouli's equation [29].

$$\begin{aligned}\Delta p = -\rho[\phi_t(x,0+) - \phi_t(x,0-) + \frac{1}{2}\{\phi_x^2(x,0+) \\ +\phi_y^2(x,0+) - \phi_x^2(x,0-) - \phi_y^2(x,0-)\}].\end{aligned} \tag{3.9}$$

Where ϕ is the velocity potential.

3.5 Unsteady Model Implementation

The overall implemented unsteady model code had the following order of operation given the user defined input parameters of step size, time step size, step size in wake, frequency, velocity at infinity, amplitude of the flap, number of the panels etc.

- Discretization of the geometry and selection of singularity elements
- Computation of influence coefficients of potential flow equation
- Kutta Condition
- Computation of influence coefficients of coupled membrane equation
- Finite difference method for membrane equation
- Enforcement of trailing edge boundary condition for $w(x,t)$
- Computation of influence coefficients for the velocity induced from wake
- Determination of vorticity distribution in the wake
- Computation of the right hand side vector of linear equations
- Solving algebraic equations for vorticity and vertical position of membrane
- Computation of pressure difference across the membrane
- Computation of horizontal forces
- Computation of net thrust and propulsive efficiency of the pump

3.5.1 Discretization of the Geometry and Selection of Singularity Elements

The total length of the steady plate, flap and membrane has been divided into N number of panels. Each panel is of the same length. A discrete vortex of vorticity $\gamma(x,t)$ has been placed at the center of each panel. Since we have used a staggered grid, the vorticity strength $\gamma(x,t)$ has been calculated at the center of each panel $(x_{i-1/2})$ where as the vertical position of membrane $w(x,t)$ has been calculated at the end point of each panel (x_i). In figure 3.2 the discretized geometry with singularity elements is shown.

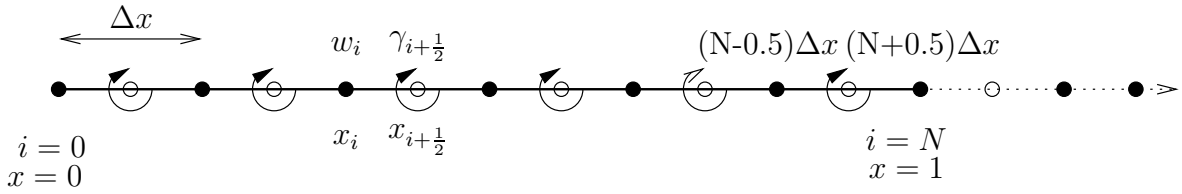

Figure 3.2: Discretized geometry with singularity elements

3.5.2 Computation of Influence Coefficients of Potential Flow Equation

First of all the coefficients of the vorticity $\gamma(x,t)$ for integral potential flow equation (2.53) have been calculated at center of each panel ($x_{j-1/2}$) where j varies from 1 to $N+1$. The coefficient matrix of the vorticity $\gamma(x,t)$ for potential flow equation (2.53) has been named HIL. For example the coefficients of jth panel has been calculated according to the following formula

$$HIl_{ij} = \frac{\delta.\Delta x}{2\sinh \pi\delta(x_i - x_j)}. \tag{3.10}$$

After this the coefficients of vertical position $w(x,t)$ for equation (2.53) have been calculated at end of the each panel (x_k) where k varies from 1 to N. The space derivative $w_x(x,t)$ has been approximated using the three point forward finite difference formula.

$$w_x = \frac{-3w(x) + 4w(x+\Delta x) - w(x+2\Delta x)}{2\Delta x}. \tag{3.11}$$

Similarly time derivative $w_t(x,t)$ have been approximated using the three point backward finite difference formula in time domain

$$w_t = \frac{3w(t) - 4w(t-\Delta t) + w(t-2\Delta t)}{2\Delta t}. \tag{3.12}$$

3.5.3 Kutta Condition

Kutta condition for unsteady flow as given by (2.58) has been applied. The time derivative of vorticity $\gamma(x,t)$ has been approximated using the three point backward finite difference formula

$$\gamma_t = \frac{3\gamma(t) - 4\gamma(t-\Delta t) + \gamma(t-2\Delta t)}{2\Delta t}. \tag{3.13}$$

3.5.4 Computation of Influence Coefficients of Coupled Membrane Equation

The influence coefficients of vorticity $\gamma(x,t)$ and vertical position $w(x,t)$ of coupled membrane equation (2.51) have been computed. For the steady rigid plate and the flap the coefficients of $\gamma(x,t)$ and $w(x,t)$ have been taken as unity. The time derivative $\gamma_t(x,t)$ at center of the panel (x_k) has been approximated using three point backward difference formula as given in equation (3.13). The integration $\int_0^x \gamma_t(\xi,t)d\xi$ has been done using mid point rule for numerical integration. For curvature of the membrane finite difference method has been applied to compute the coefficients of $w(x,t)$.

Finite Difference Method for Membrane Equation

The pressure difference across the membrane is given in equation (2.23). To approximate the second derivative finite difference method has been applied. A uniform mesh with uniform spacing Δx has been used. For interval $0 \leq x \leq 1$ the spacing would be $\Delta x = \frac{1}{N+1}$, and the mesh points would be

$$x_i = i\Delta x, i = 0, ..., N+1. \tag{3.14}$$

The second derivative has been approximated by using three point centered second order finite difference formula

$$w_{xx} = \frac{w_{x+\Delta x} - 2w + w_{x+\Delta x}}{(\Delta x)^2}. \tag{3.15}$$

3.5.5 Enforcement of Trailing Edge Boundary Condition

The trailing edge boundary condition for $w(x,t)$ has been applied as follows

$$w_t + \frac{1}{Sr}(w_x) = 0. \tag{3.16}$$

The space derivative w_x has been approximated using backward difference formula

$$w_x = \frac{3w(x) - 4w(x-\Delta x) + w(x-2\Delta x)}{2\Delta x}. \tag{3.17}$$

The time derivative w_t has been approximated using the following finite difference formula

$$w_t = \frac{w(t) - w(t-\Delta t)}{2\Delta t}. \tag{3.18}$$

3.5.6 Computation of Influence Coefficients for the Velocity Induced from Wake

The number of wake points are taken as NW. The step size in the wake has been taken as $\Delta x_w = \Delta t/Sr$, where Δt is the time step size and Sr is the Strouhal number. The coordinate of the vortices in the wake have been computed as

$$x_{w,j} = 1.0 + \Delta x/2 + j\Delta x_w. \tag{3.19}$$

where j varies from 1 to NW. The coefficients of vorticity strength $\gamma_w(x,t)$ have been calculated and the coefficient matrix for wake induced velocities HW has been build. The coefficients of the matrix HW have been approximated using the following formula

$$HW_{ij} = \frac{\delta.\Delta x_w}{2\sinh \pi\delta(x_i - x_{w,j})}. \tag{3.20}$$

3.5.7 Determination of Vorticity Distribution in the Wake

Along the vortices on the physical geometry there are vortices shed in the wake. For NW wake points vorticity distribution in the wake is computed using the upwind scheme.

$$\gamma_{w,i} = \gamma_{w,i}(1 - \frac{\Delta t}{\Delta x_w Sr}) + \gamma_{w,i-1}(1 - \frac{\Delta t}{\Delta x_w Sr}). \tag{3.21}$$

3.5.8 Computation of the Right Hand Side Vector of Linear Equations

After computation of the influence coefficients matrices the right hand side vector of linear equations set have been set up.

Velocity induced from the Wake

The velocity induced from the wake has been calculated using the influence coefficient matrix HW and the vorticity induced from the wake which has been computed in equation (3.21).

Motion of flap

The flap which excites the membrane have been moved sinusoidally up and down according to the formula

$$w(x_m, t) = \sin(2\pi t). \tag{3.22}$$

To avoid the initial jerk motion of the flap have been kept smooth initially according to the following formula

$$w(x_m, t) = Ct^2(t - \frac{1}{2}). \tag{3.23}$$

After calculating constant C, the motion of the flap has been prescribed like

$$w(x_m, t) = \begin{cases} -8\pi t^2(t - \frac{1}{2}) & : \quad 0 \leq t \leq \frac{1}{2}, \\ \sin(2\pi t) & : \quad t > \frac{1}{2}. \end{cases} \tag{3.24}$$

3.5.9 Solving Algebraic Equations for Vorticity and Vertical Position of Membrane

After building all the coefficient matrices and the right hand side vector. The system of equations to be solved is

$$\begin{pmatrix} A_{1,1} & \dots & A_{1,j} & \dots & A_{1,2N+1} \\ \vdots & \ddots & \vdots & \ddots & \vdots \\ A_{i,1} & \dots & A_{i,j} & \dots & A_{i,2N+1} \\ \vdots & \ddots & \vdots & \ddots & \vdots \\ A_{2N+1,1} & \dots & A_{2N+1,j} & \dots & A_{2N+1,2N+1} \end{pmatrix} \begin{pmatrix} \gamma_1 \\ w_1 \\ \vdots \\ w_{2N} \\ \gamma_{2N+1} \end{pmatrix} = \begin{pmatrix} RHS_1 \\ RHS_2 \\ \vdots \\ RHS_{2N} \\ RHS_{2N+1} \end{pmatrix}. \tag{3.25}$$

This system of equations has been solved using a standard linear solver.

3.5.10 Computation of Pressure Difference Across the Membrane

After solving the algebraic equations we have the vorticity $\gamma(x, t)$ and the vertical position of membrane $w(x, t)$. From this vorticity we can calculate the total circulation. The total circulation Γ_t at instant time t is given as

$$\Gamma_t = \int_0^x \gamma(x, t)dx. \tag{3.26}$$

Here the numerical integration has been done using mid point rule. Similarly we can calculate circulations $\Gamma_{t-\Delta t}$ at instant time $(t - \Delta t)$ and $\Gamma_{t-2\Delta t}$ at instant time $(t - 2\Delta t)$ respectively. Now from these circulations we can calculate the pressure difference across the membrane using three point finite difference formula. The pressure difference across the membrane at each time step is given as

$$\Delta p = \frac{(1.5\Gamma_t - 2.0\Gamma_{t-\Delta t} + 0.5\Gamma_{t-2\Delta t})}{\Delta t} + \frac{1.0}{Sr}\gamma_t. \tag{3.27}$$

3.5.11 Computation of Horizontal Forces

After calculating the pressure difference across the membrane we can calculate the horizontal component of the pressure force on the steady plate, flap and membrane. We first calculate the slope for the vertical position w_x.

$$w_x = \Delta w/\Delta x. \tag{3.28}$$

Using equation (2.63) the horizontal pressure force can be calculated. The leading edge thrust can be approximated from equation (2.64).

3.5.12 Computation of Net Thrust and Efficiency of the Pump

The net thrust of the pump is sum of the horizontal component of the pressure force and the leading edge thrust. Therefore the net thrust of the pump can be found by adding horizontal pressure force and leading edge thrust.

$$F = F_p + F_{le}. \tag{3.29}$$

The propulsive efficiency of the pump is ratio of the net thrust to the power input. To calculate the power required to maintain the motion we first calculate the time derivative of vertical position w_t.

$$w = \Delta w/\Delta t. \tag{3.30}$$

Then the input power is calculated using equation (2.66). Finally using equation (2.69) efficiency of the propulsion of the pump can be calculated.

3.6 Error Estimation Using Richardson's Extrapolation

The accuracy of the net horizontal forces improves when we increase the number of panel. However we can not increase the number of panels over a certain value due to computational restrictions. Therefore we extrapolate here the horizontal forces using Richardson's extrapolation formula [4]. Richardson's formula for estimation of error is given as

$$F_N - F \sim \frac{C_1}{N^{1/2}} + \frac{C_2}{N} + \frac{C_3}{N^{3/2}} + ... \tag{3.31}$$

We approximate here for N, $2N$, $4N$ and $8N$ and neglect the higher order terms so

$$F_N - F \sim \frac{C_1}{N^{1/2}} + \frac{C_2}{N} + \frac{C_3}{N^{3/2}} \tag{3.32}$$

$$F_{2N} - F \sim \frac{C_1}{(2N)^{1/2}} + \frac{C_2}{2N} + \frac{C_3}{(2N)^{3/2}} \tag{3.33}$$

$$F_{4N} - F \sim \frac{C_1}{(4N)^{1/2}} + \frac{C_2}{4N} + \frac{C_3}{(4N)^{3/2}} \tag{3.34}$$

$$F_{8N} - F \sim \frac{C_1}{(8N)^{1/2}} + \frac{C_2}{8N} + \frac{C_3}{(8N)^{3/2}} \tag{3.35}$$

Solving the above four equations we can find the value of F which is the required extrapolated value of net thrust. The estimated error in the net thrust is shown in table 3.1.

3.7 Selection of Number of Panels

In order to select appropriate number of panels an analysis has been performed. The dimensionless constants α, β, Sr and δ have been calculated and in table 2.3 their values are given. These constants remain same while the number of panels have been changed from 20 to 2400. Results for the all the horizontal forces for the different number of panels are shown in the table 3.1, figure 3.3 and figure 3.4. According to these figures when the number of panels reached 600 or more, there is not much change in the forces. Also the vertical position of the membrane $w(x,t)$ was calculated and a graph of $w(x,t)$ against x position at $t = 50.9975$ was drawn for different panels. As it is obvious from the figure 3.5, $w(x,t)$ does not change much when the number of panels is 600 or above 600. Similarly vorticity $\gamma(x,t)$ was calculated and a graph of $\gamma(x,t)$ against x position at time $t = 50.9975$ was drawn for different panels. It is clear from figure 3.6 that $\gamma(x,t)$ does not change much when the number of panels is 600 or above 600. So 600 was selected as the appropriate number of panels. All the later simulations have been done using 600 as number of panels.

3.8 Selection of Number of Points in the Wake

To select the number of points in the wake simulations with constants α, β, Sr and δ as shown in the table 2.3 have been investigated. The number of points in the wake have been increased from 1000 to 4000. It was observed that increasing the number of points in wake does not have much difference on the vorticity and the vertical position of the membrane as shown in the figures (3.7), (3.10), (3.8), (3.11), (3.9), (3.12). So the number of points in the wake were taken as 1000 for all the later simulations.

Table 3.1: Sensitivity of horizontal forces to the number of panels

No. Of Panels (N)	Horizontal Force (F_p)	Leading Edge Thrust (F_{le})	Net Thrust (F)	Estimated Error
20	-5.9403	-0.48310	-6.4234	4.2874
50	-2.7162	-0.22310	-2.9393	0.8033
100	-2.3192	-0.15800	-2.4772	0.3412
200	-2.1949	-0.11680	-2.3117	0.1757
300	-2.1639	-0.09730	-2.2612	0.1252
400	-2.1502	-0.08800	-2.2382	0.1022
500	-2.1424	-0.07920	-2.2216	0.0856
600	-2.1374	-0.07620	-2.2136	0.0776
800	-2.1312	-0.07060	-2.2018	0.0658
1000	-2.1272	-0.06580	-2.1930	0.0570
1200	-2.1244	-0.06270	-2.1871	0.0511
1600	-2.1206	-0.05890	-2.1795	0.0435
2400	-2.1163	-0.05400	-2.1703	0.0343

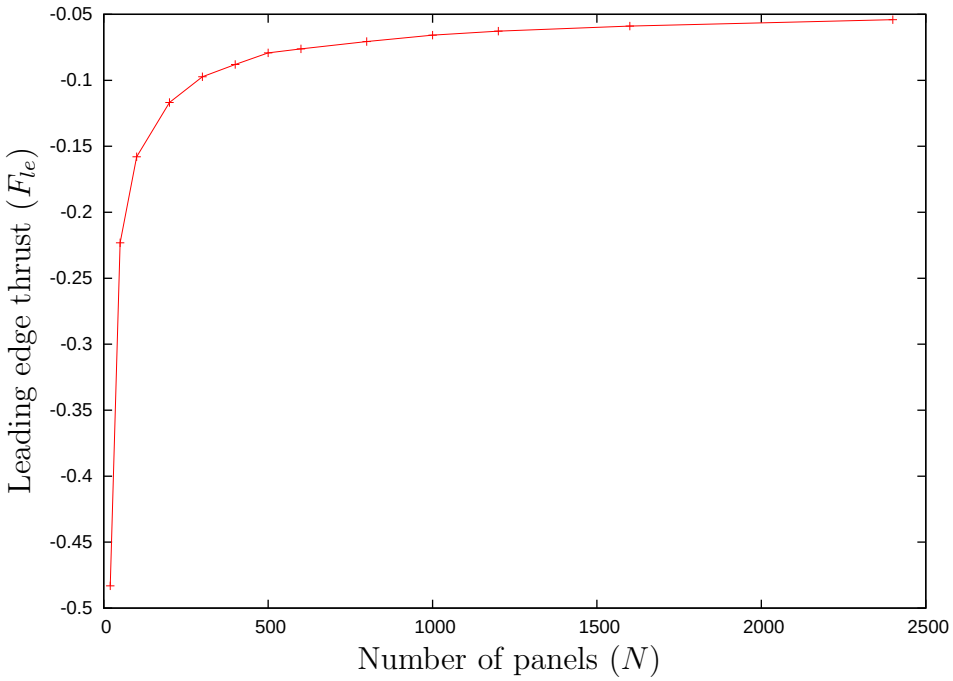

Figure 3.3: Leading edge thrust for different number of panels

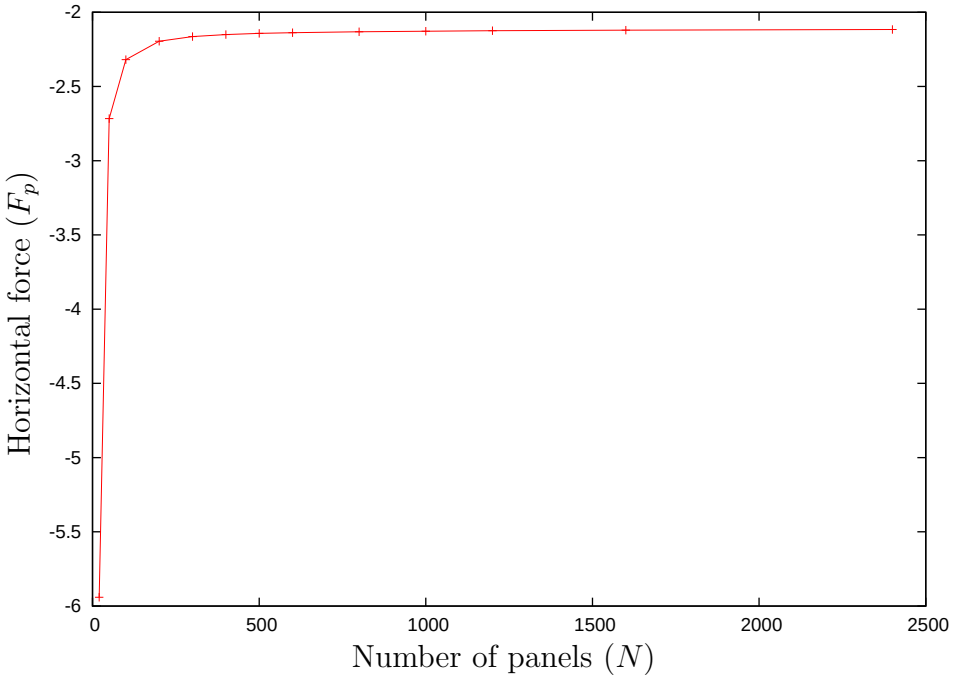

Figure 3.4: Horizontal pressure force for different number of panels

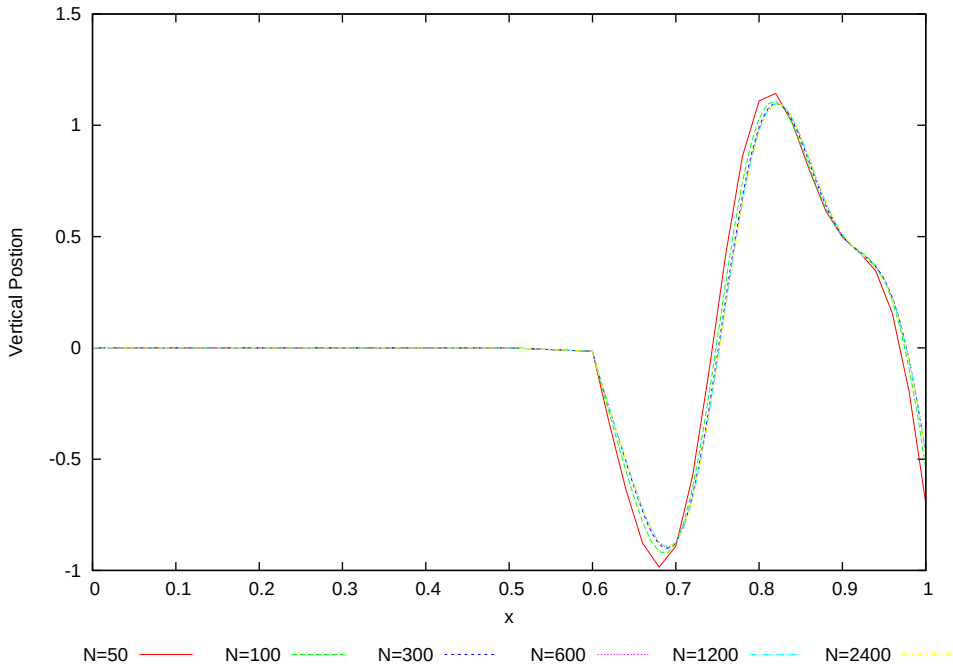

Figure 3.5: Comparison of vertical position for different number of panels after 50 periods at $t = 50.9975$

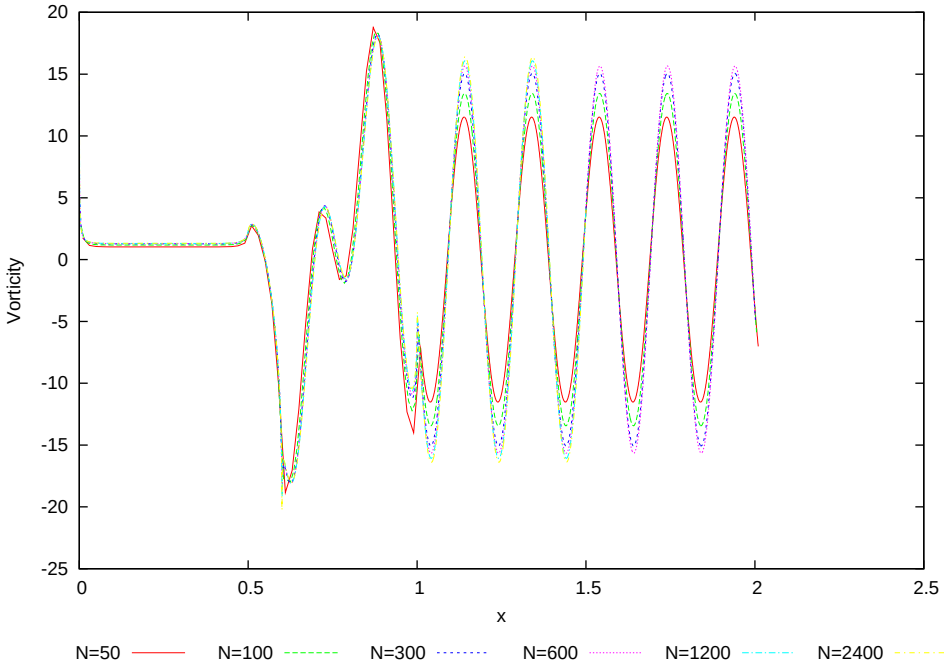

Figure 3.6: Comparison of vorticity for different number of panels after 50 periods at $t = 50.9975$

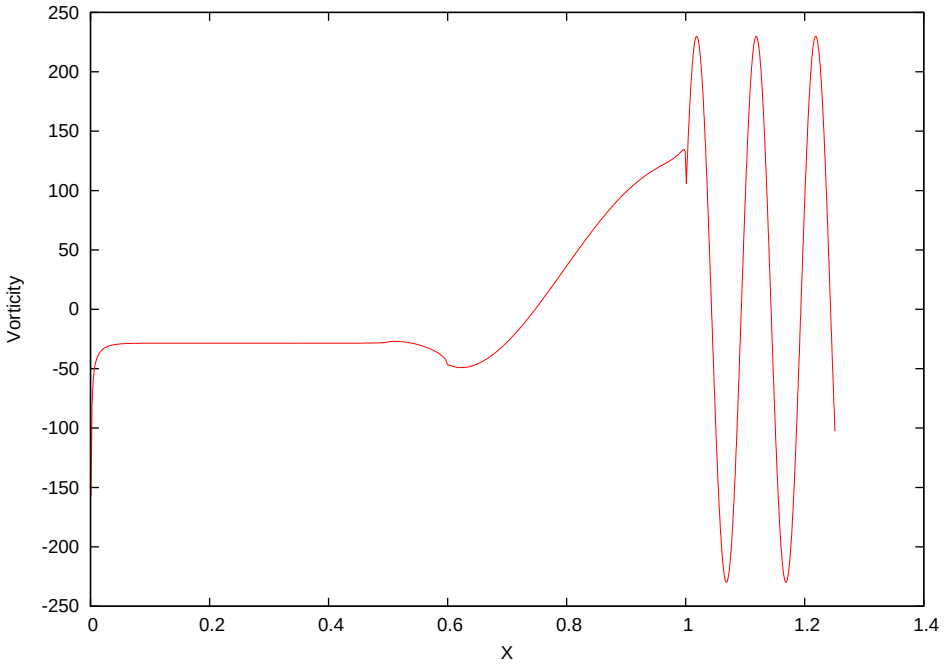

Figure 3.7: Vorticity for 1000 number of wake points at $t = 50.9975$

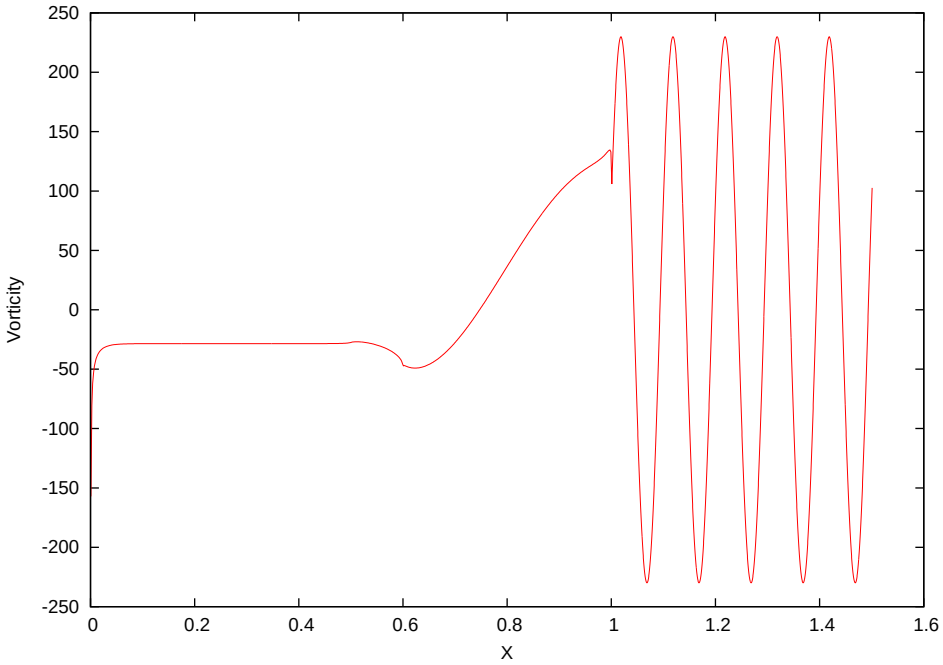

Figure 3.8: Vorticity for 2000 number of wake points at $t = 50.9975$

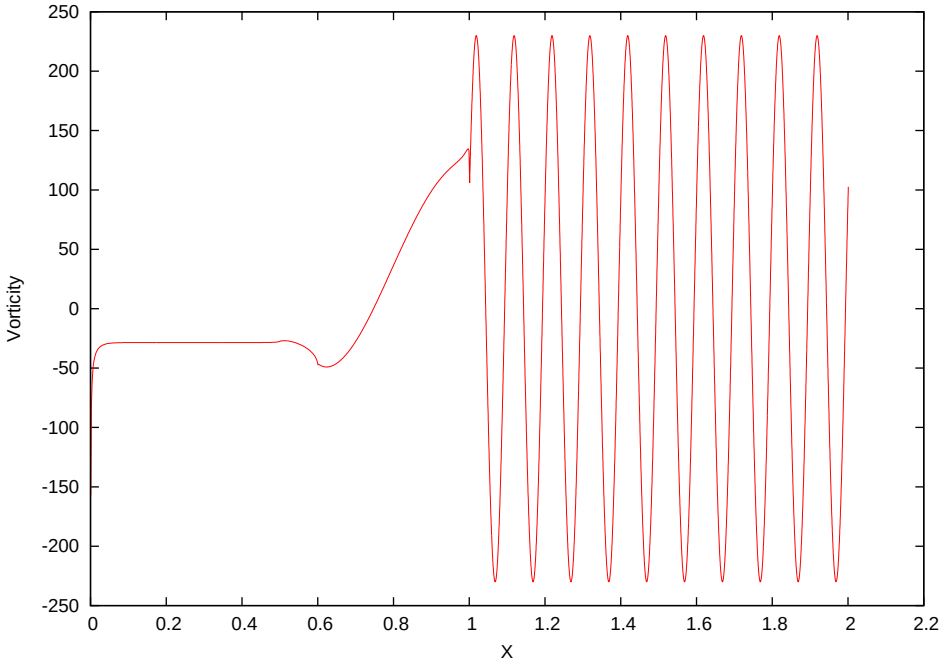

Figure 3.9: Vorticity for 4000 number of wake points at $t = 50.9975$

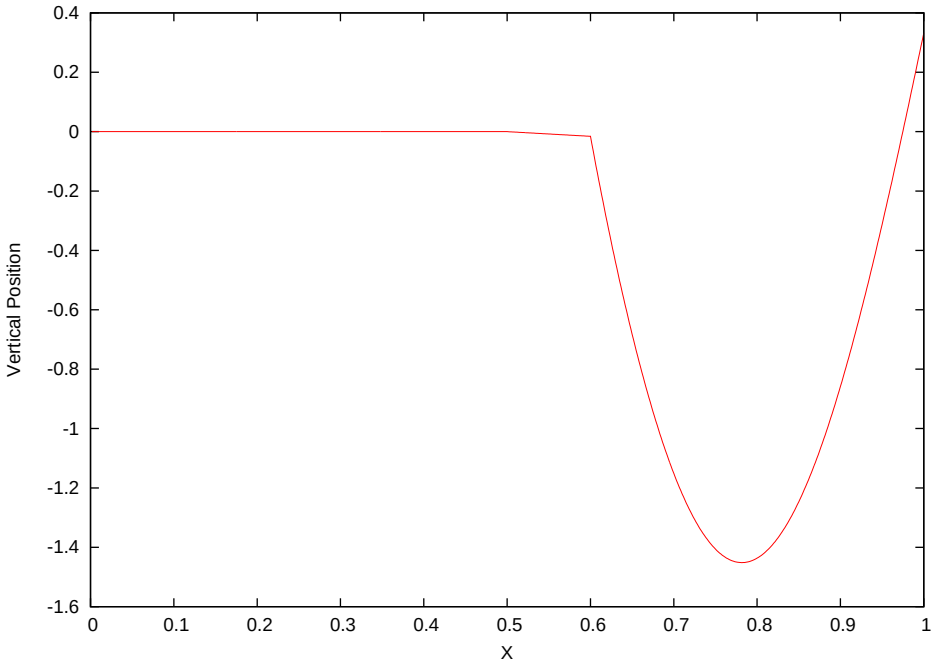

Figure 3.10: Vertical position of membrane for 1000 number of wake points at $t = 50.9975$

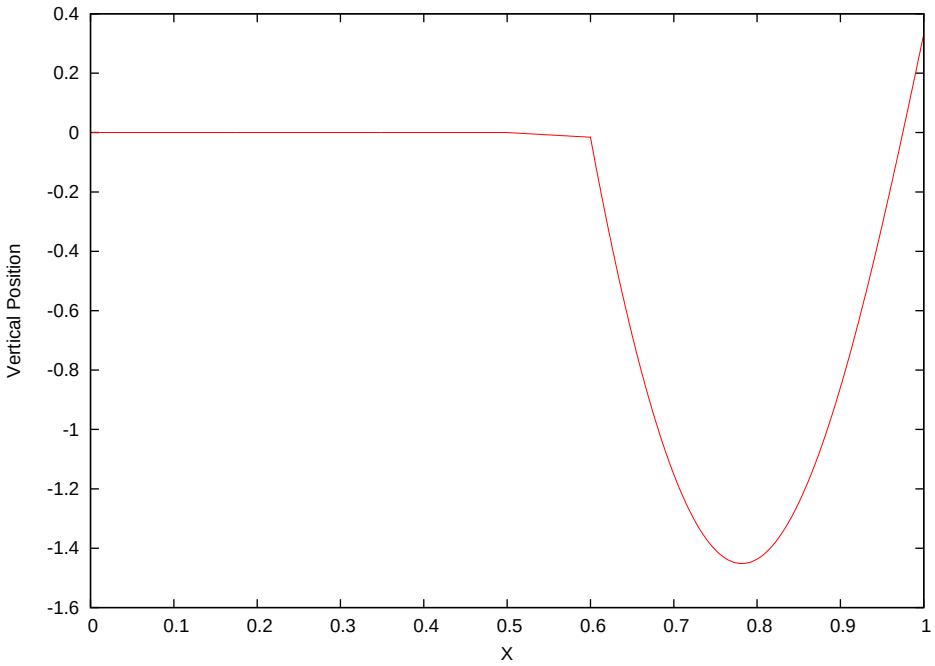

Figure 3.11: Vertical position of membrane for 2000 number of wake points at $t = 50.9975$

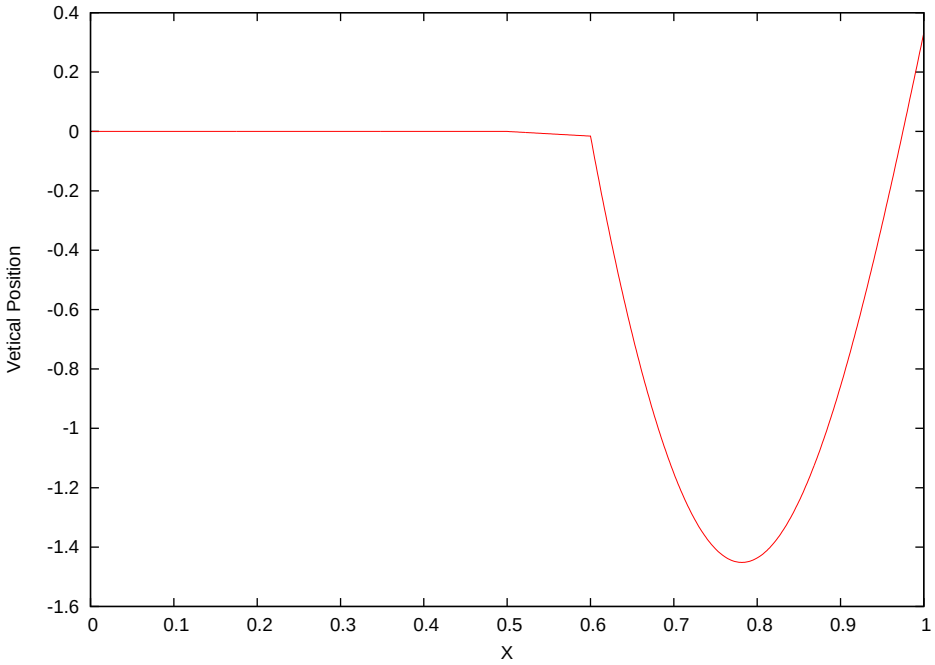

Figure 3.12: Vertical position of membrane for 4000 number of wake points at $t = 50.9975$

Chapter 4

Results

In this chapter the results obtained have been analyzed. Number of panels for the plate, flap and membrane are fixed at 600 for all the simulations.

4.1 Variation of Strouhal number keeping $\beta = 0.00963$ and $\delta = 5.0$

In this section length to width ratio of the channel has been kept small as $\delta = 5.0$. The tensions in the membrane have been taken from Zackl,s report [77]. Therefore the dimensionless constants calculated are $\alpha = 1.2323$ and $\beta = 0.00963$. Vertical position of the membrane after 50 periods at $t = 50.0$ (flap is at its mean position), $t = 50.25$ (flap is at extreme position in upward direction), $t = 50.75$ (flap is at extreme position in downward direction) is shown in figure 4.1. In figure 4.2 vertical positions of membrane at time $t = 50.0$ (when the flap is at its mean position) for different Strouhal numbers have been compared. We can see that motion of the membrane has maximum amplitude when $Sr = 10$. The amplitude of the membrane increases by increasing the Strouhal number until a certain value and then it decreases. In figure 4.3 the vorticities on the membrane and in the wake at time $t = 50.0$ (when the flap is at its mean position) for different Strouhal numbers have been compared. The vorticity has the maximum value for $Sr = 10.0$. In figures 4.4 and 4.6 the vertical positions of the membrane at $t = 50.25$ and $t = 50.75$ for different Strouhal numbers are compared. Similarly in figures 4.5 and 4.7 the vorticities at $t = 50.25$ and $t = 50.75$ for different Strouhal numbers have been compared. It is evident from these figures that the vorticity increases by increasing the Strouhal number until a certain value of Strouhal number and then it decreases. In table 4.1 periodic horizontal pressure force and the leading edge thrust are shown for different

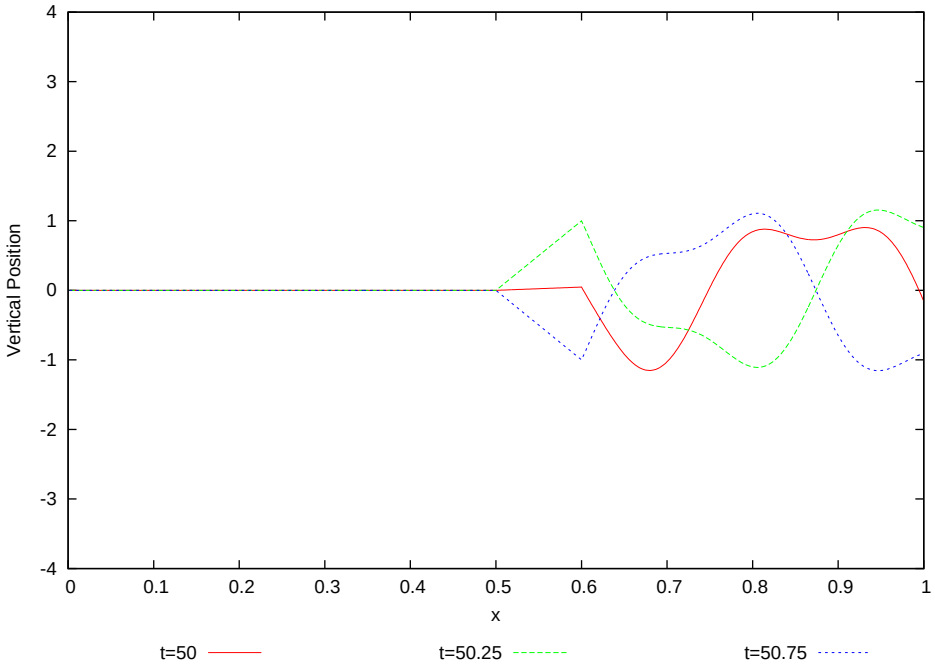

Figure 4.1: Vertical position at $t = (50.0, 50.25, 50.75)$, for $Sr = 5.0$, $\beta = 0.00963$, and $\delta = 5.0$

Strouhal numbers keeping $\delta = 5.0$ and $\beta = 0.00963$. We can see from the table that horizontal forces have maximum values at $Sr = 10.0$.

4.2 Variation of Strouhal number keeping $\beta = 0.00963$ and $\delta = 10.0$

In this section width of channel has been decreased so the length to width ratio of the channel have been kept as $\delta = 10.0$. The tensions in the membrane have been kept same as in the previous case so the dimensionless constants $\alpha = 1.2323$ and $\beta = 0.00963$. Vertical position of the membrane after 50 periods at $t = 50.0$ (flap is at its mean position), $t = 50.25$ (flap is at extreme position in upward direction) and $t = 50.75$ (flap is at extreme position in downward direction) is shown in figure 4.8. In figure 4.9 the vertical position of membrane at $t = 50.0$ (when the flap is at its mean position) for different Strouhal numbers have been compared. It is clear from this figure that by increasing the Strouhal number the amplitude of the membrane motion increases until $Sr = 20$ and then there is not much change in the amplitude of the motion of the membrane by increasing the Strouhal number. In fig-

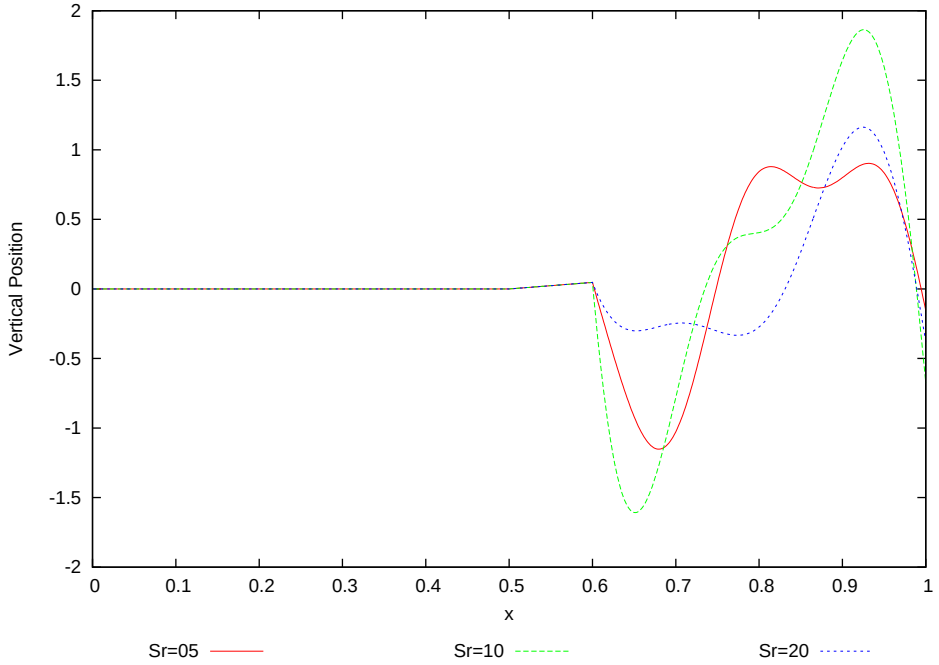

Figure 4.2: Comparison of the vertical position at $t = 50.0$, for $Sr = (5.0, 10.0, 20.0)$, $\beta = 0.00963$ and $\delta = 5.0$

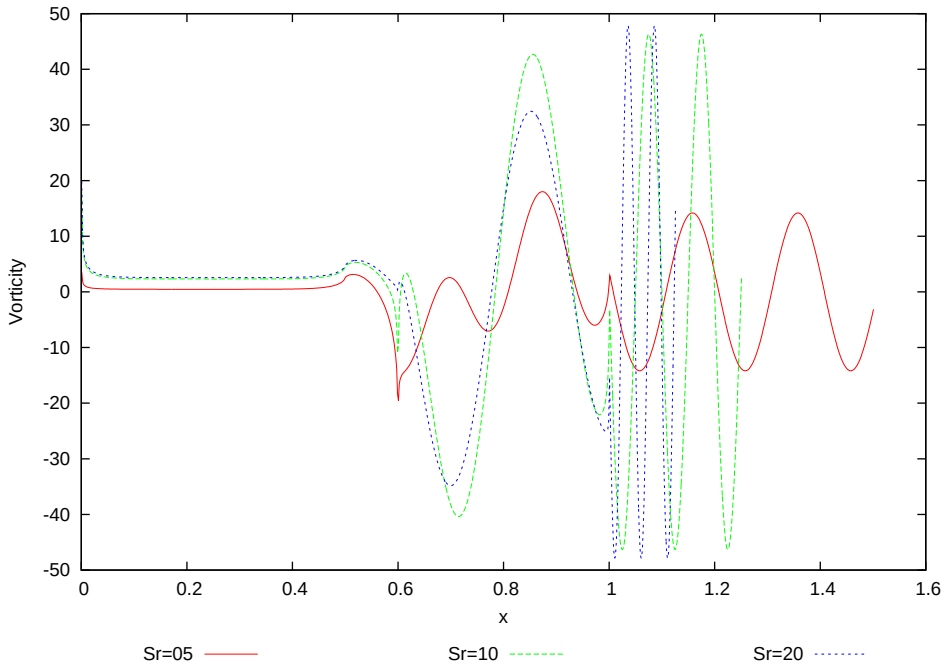

Figure 4.3: Comparison of the vorticity at $t = 50.0$, for $Sr = (5.0, 10.0, 20.0)$, $\beta = 0.00963$ and $\delta = 5.0$

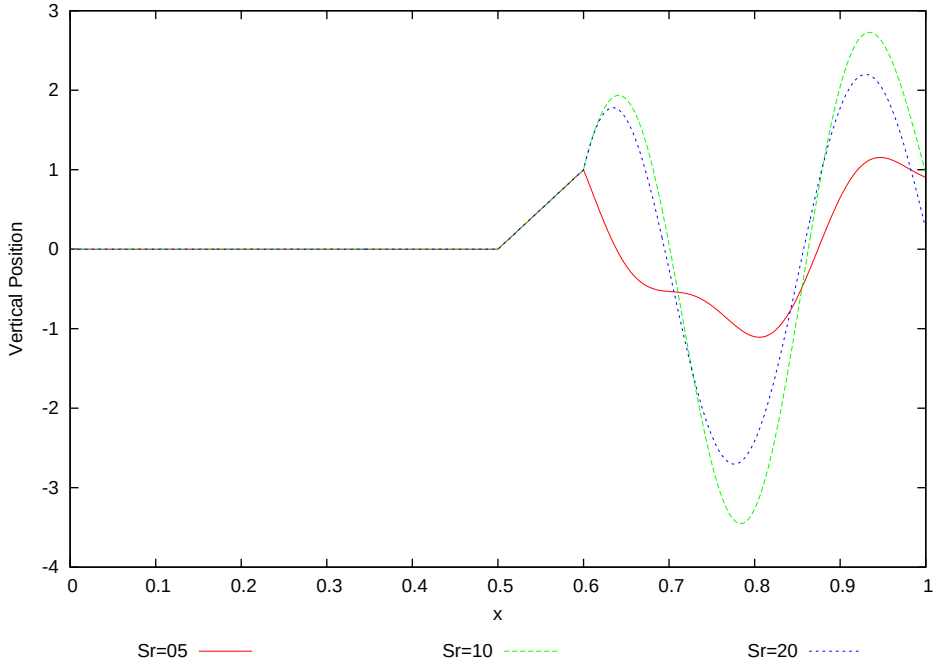

Figure 4.4: Comparison of the vertical position at $t = 50.25$, for $Sr = (5.0, 10.0, 20.0)$, $\beta = 0.00963$ and $\delta = 5.0$

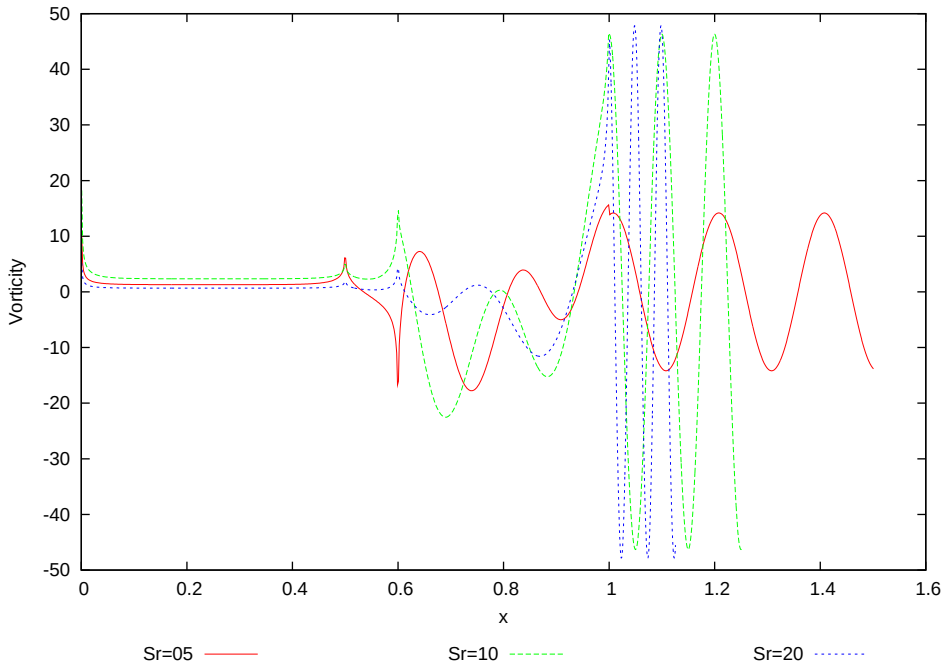

Figure 4.5: Comparison of the vorticity at $t = 50.25$, for $Sr = (5.0, 10.0, 20.0)$, $\beta = 0.00963$ and $\delta = 5.0$

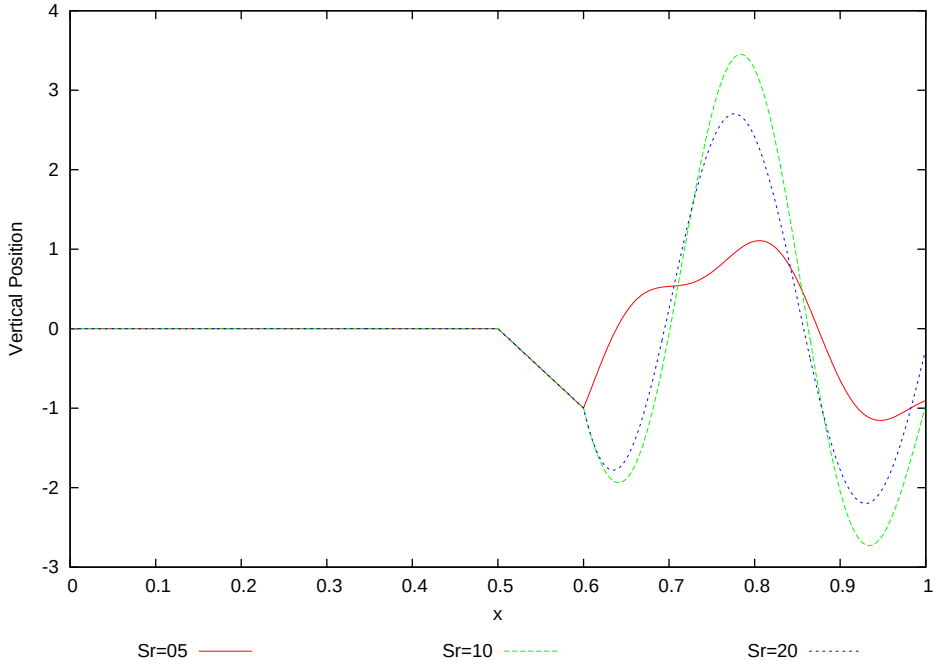

Figure 4.6: Comparison of the vertical position at $t = 50.75$, for $Sr = (5.0, 10.0, 20.0)$, $\beta = 0.00963$ and $\delta = 5.0$

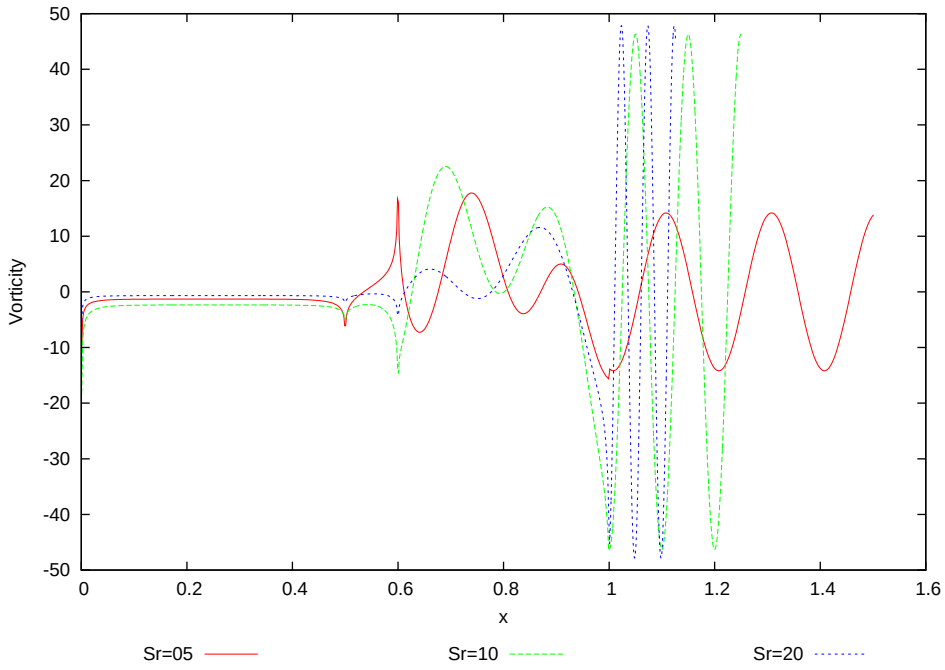

Figure 4.7: Comparison of the vorticity at $t = 50.75$, for $Sr = (5.0, 10.0, 20.0)$, $\beta = 0.00963$ and $\delta = 5.0$

Table 4.1: Horizontal forces for different Strouhal numbers at $\alpha = 1.2323$, $\beta = 0.00963$ and $\delta = 5.0$

Strouhal Number (Sr)	Horizontal Force (F_p)	Leading Edge Thrust (F_{le})
5.0	-1.798295	-0.036411
10.0	-6.5248624	-0.208941
20.0	-3.2276032	-0.133994
100.0	-2.2890366	-0.095691

Table 4.2: Horizontal forces for different Strouhal numbers at $\alpha = 1.2323$, $\beta = 0.00963$ and $\delta = 10.0$

Strouhal Number (Sr)	Horizontal Force (F_p)	Leading Edge Thrust (F_{le})
5.0	-2.1374366	-0.07629770
10.0	-5.5628758	-0.07678598
20.0	-18.900380	-0.33576209
100.0	-82.267114	-1.6535522

ure 4.10 the vorticities on the membrane and in the wake at $t = 50.9975$ for different Strouhal numbers have been compared. The vorticity increases monotonically by increasing the Strouhal number. In table 4.2 periodic horizontal force and the leading edge thrust are shown for different Strouhal numbers keeping $\delta = 10.0$ and $\beta = 0.00963$. It is evident from the table 4.2 that increasing the Strouhal number we get higher net horizontal forces.

4.3 Variation of Strouhal number keeping $\beta = 0.00963$ and $\delta = 20.0$

In this section width of channel has been further decreased so the length to width ratio of the channel has been kept as $\delta = 20.0$. The tensions in the membrane have been kept same as in the previous case so the dimensionless constants $\alpha = 1.2323$ and $\beta = 0.00963$. Vertical position of the membrane after 50 periods at $t = 50.0$, $t = 50.25$, $t = 50.75$ and $t = 50.9975$ is shown in figure 4.11. In figure 4.12 the vertical positions of membrane at $t = 50.0$ (when the flap is at its mean position) for different Strouhal numbers

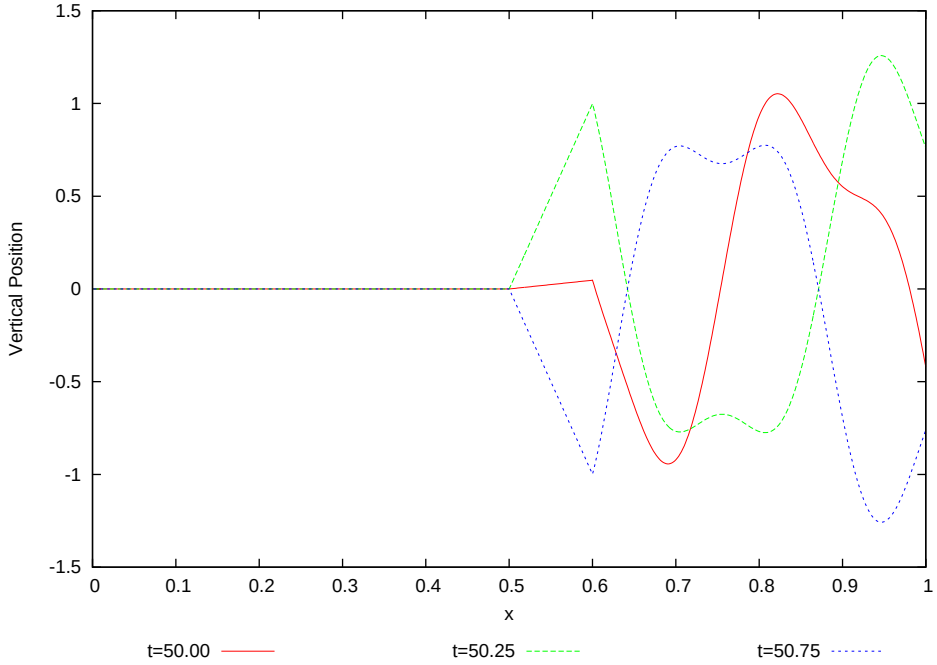

Figure 4.8: Vertical position at $t = (50.0, 50.25, 50.75)$, for $Sr = 5.0$, $\beta = 0.00963$ and $\delta = 10.0$

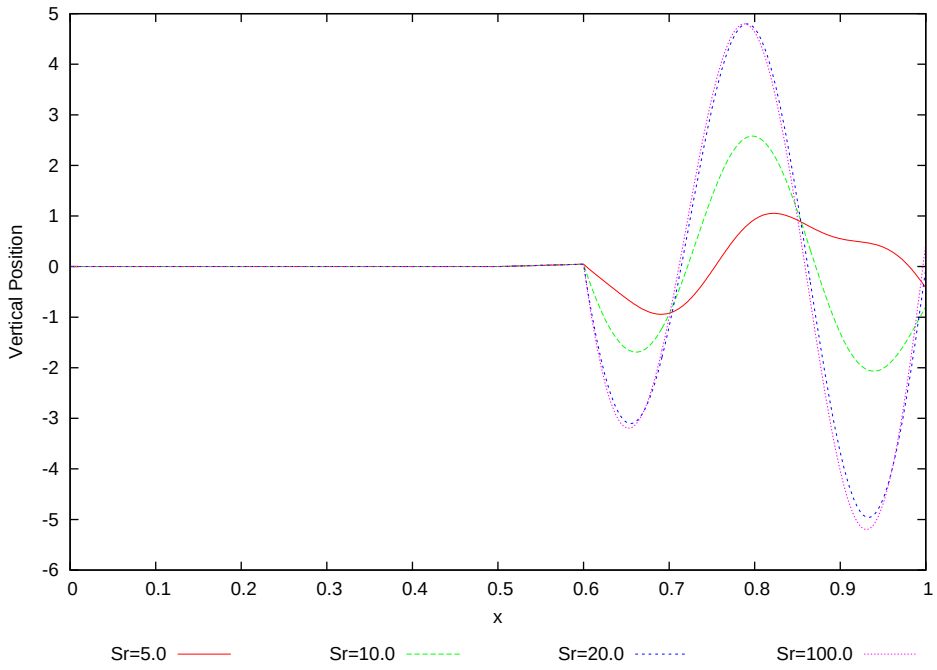

Figure 4.9: Comparison of the vertical position at $t = 50.0$, for $Sr = (5.0, 10.0, 20.0, 100.0)$, $\beta = 0.00963$ and $\delta = 10.0$

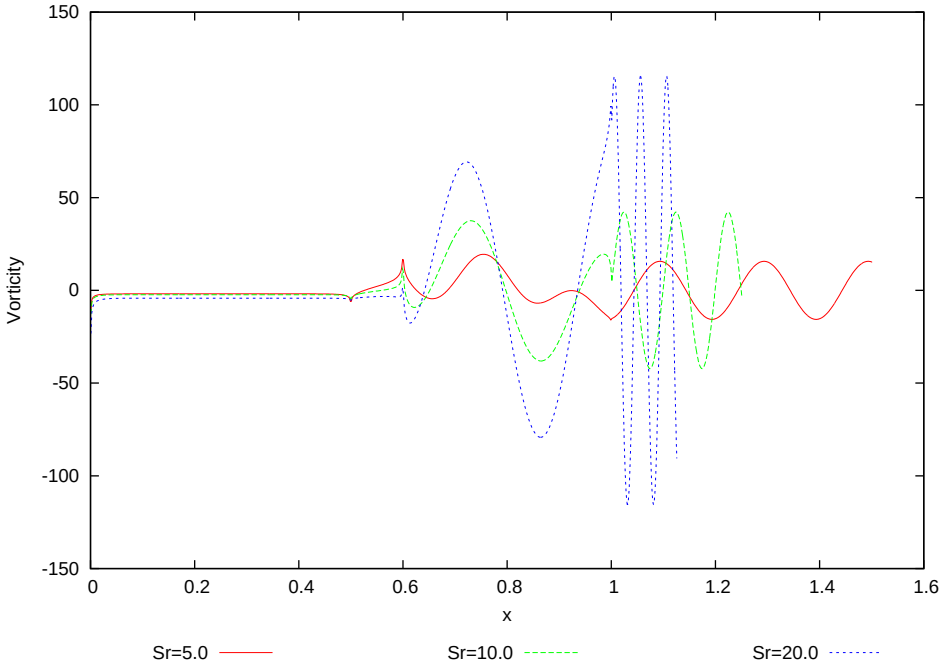

Figure 4.10: Comparison of the vorticity at $t = 50.9975$, for $Sr = (5.0, 10.0, 20.0)$, $\beta = 0.00963$ and $\delta = 10.0$

have been compared. In this case we see increasing the Strouhal number the amplitude of the membrane motion decreases contrary to the previous cases. In figure 4.13 the vorticities on the membrane and in the wake at $t = 50.9975$ for different Strouhal numbers have been compared. In table 4.3 periodic horizontal force and the leading edge thrust are shown for different Strouhal numbers keeping $\delta = 20.0$ and $\beta = 0.00963$. The table 4.3 shows that increasing the Strouhal number we get less net horizontal forces. This reverse behavior is due to the high aspect ratio. The channel should not be too narrow to get better efficiency.

4.4 Variation of Strouhal number keeping $\beta = 0.9630$ and $\delta = 5.0$

In this section width of channel has been kept large which means low aspect ratio $\delta = 5.0$. The tensions in the membrane have been increased. The dimensionless constant α was kept same as in the previous cases where as the value of β was increased. Vertical position of the membrane after 50 periods at $t = 50.0$, $t = 50.25$, $t = 50.75$ and $t = 50.9975$ is shown in figure

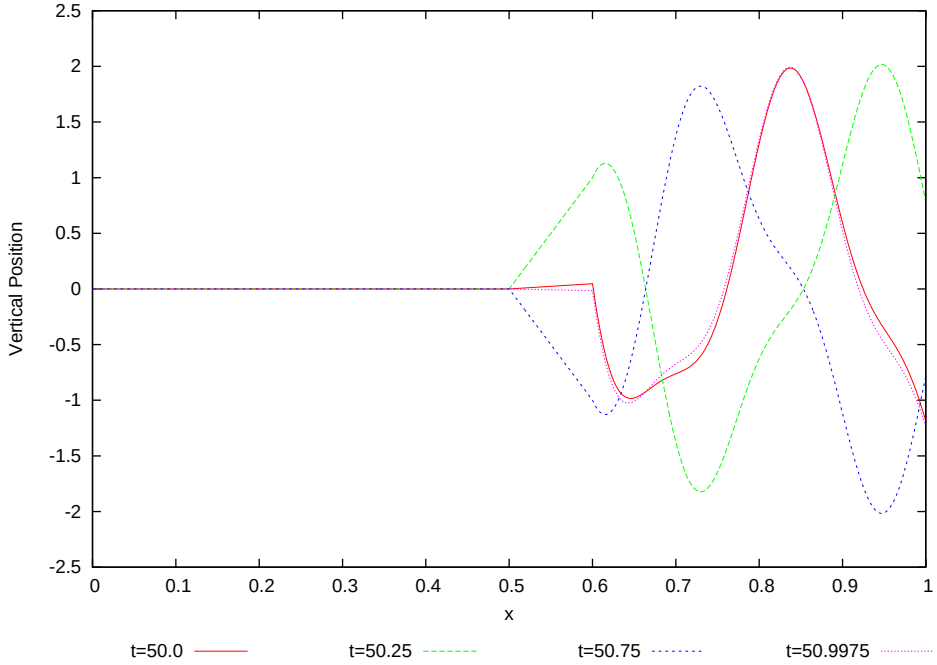

Figure 4.11: Vertical position at $t = (50.0, 50.25, 50.75, 50.9975)$, for $Sr = 5.0$, $\beta = 0.00963$ and $\delta = 20.0$

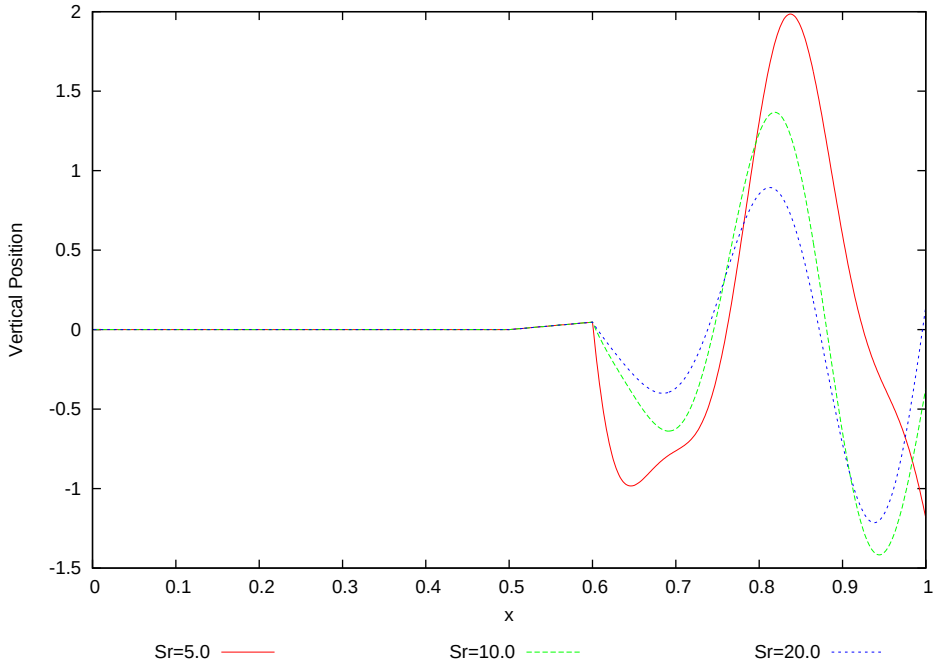

Figure 4.12: Comparison of the vertical position at $t = 50.0$, for $Sr = (5.0, 10.0, 20.0)$, $\beta = 0.00963$ and $\delta = 20.0$

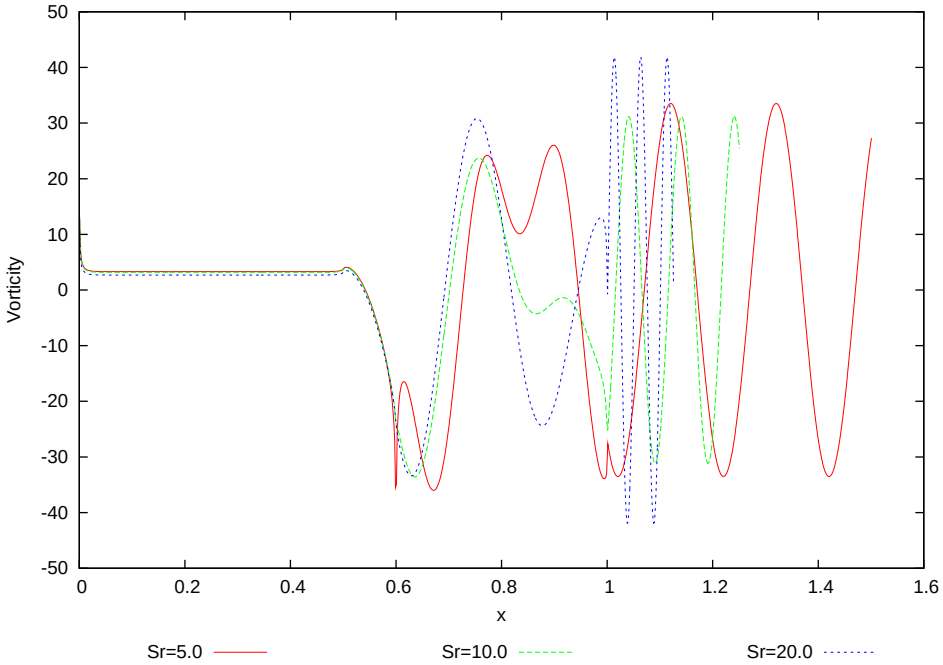

Figure 4.13: Comparison of the vorticity at $t = 50.9975$, for $Sr = (5.0, 10.0, 20.0)$, $\beta = 0.00963$ and $\delta = 20.0$

Table 4.3: Horizontal forces for different Strouhal numbers at $\alpha = 1.2323$, $\beta = 0.00963$ and $\delta = 20.0$

Strouhal Number (Sr)	Horizontal Force (F_p)	Leading Edge Thrust (F_{le})
5.0	-7.8345709	-0.48526679
10.0	-2.9180772	-0.16469291
20.0	-2.4917719	-0.09715820
100.0	-2.2168028	-0.07194497

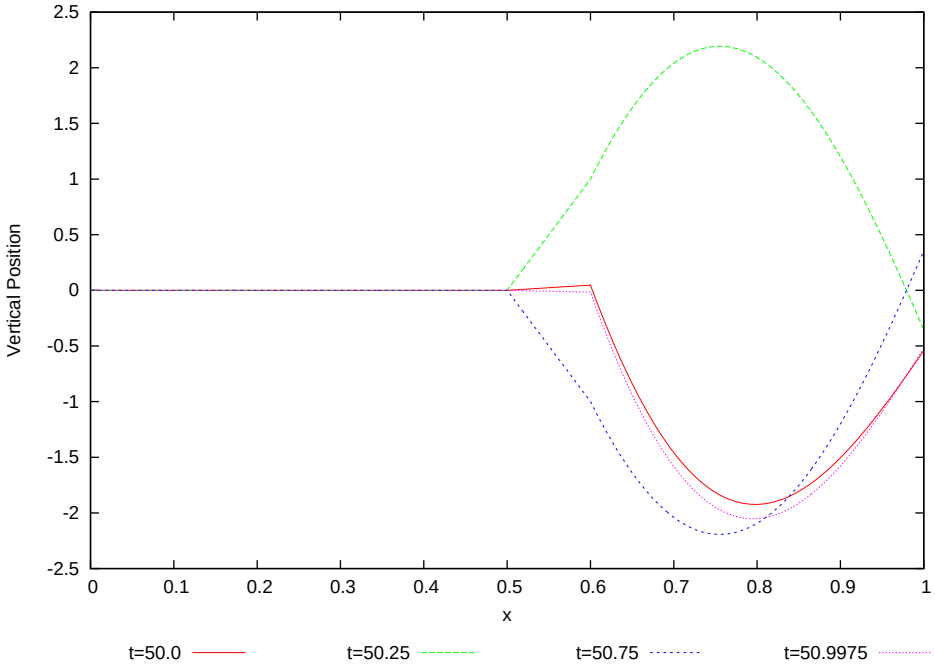

Figure 4.14: Vertical position at $t = (50.0, 50.25, 50.75, 50.9975)$, for $Sr = 5.0$, $\beta = 0.9630$ and $\delta = 5.0$

4.14. In figure 4.15 the vertical positions of membrane at time $t = 50.0$ (when the flap is at its mean position) for different Strouhal numbers have been compared. In figure 4.16 the vorticities on the membrane and in the wake at time $t = 50.25, t = 50.75$ for different Strouhal numbers, $Sr = 5.0$ have been plotted. In figure 4.17 the vorticities on the membrane and in the wake at $t = 50.9975$ for different Strouhal numbers have been compared. It is evident that the vorticity increases by increasing the Strouhal number. In table 4.4 periodic horizontal force and the leading edge thrust are shown for different Strouhal numbers keeping $\delta = 5.0$ and $\beta = 0.9630$. We can see from the table 4.4 that the periodic horizontal forces increase by increasing the Strouhal number until $Sr = 20.0$ and then the horizontal forces start decreasing. So the optimum value of the Strouhal number in this case is $Sr = 20.0$.

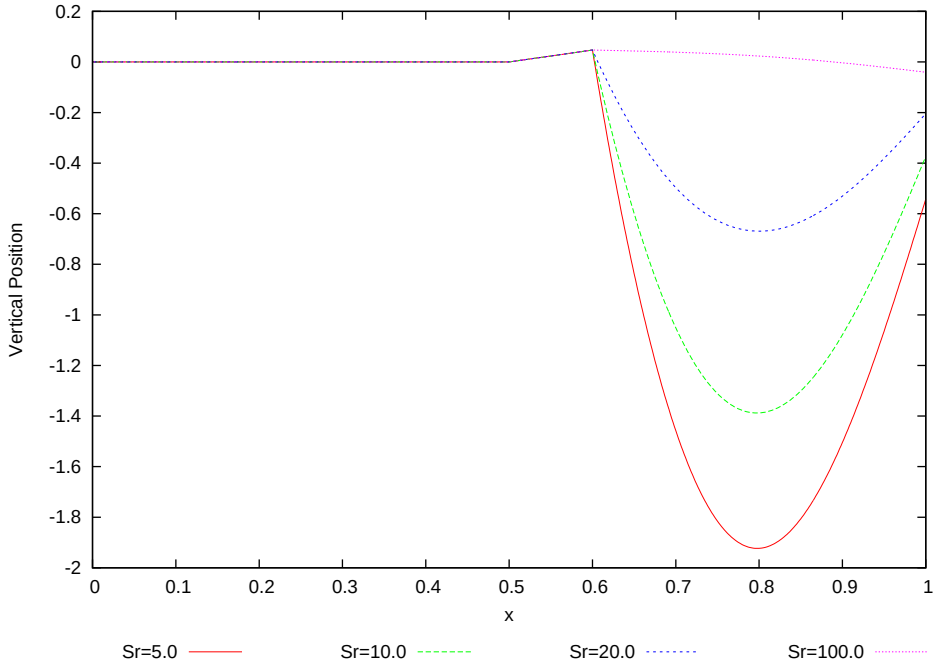

Figure 4.15: Comparison of the vertical position at $t = 50.0$, for $Sr = (5.0, 10.0, 20.0, 100.0)$, $\beta = 0.9630$ and $\delta = 5.0$

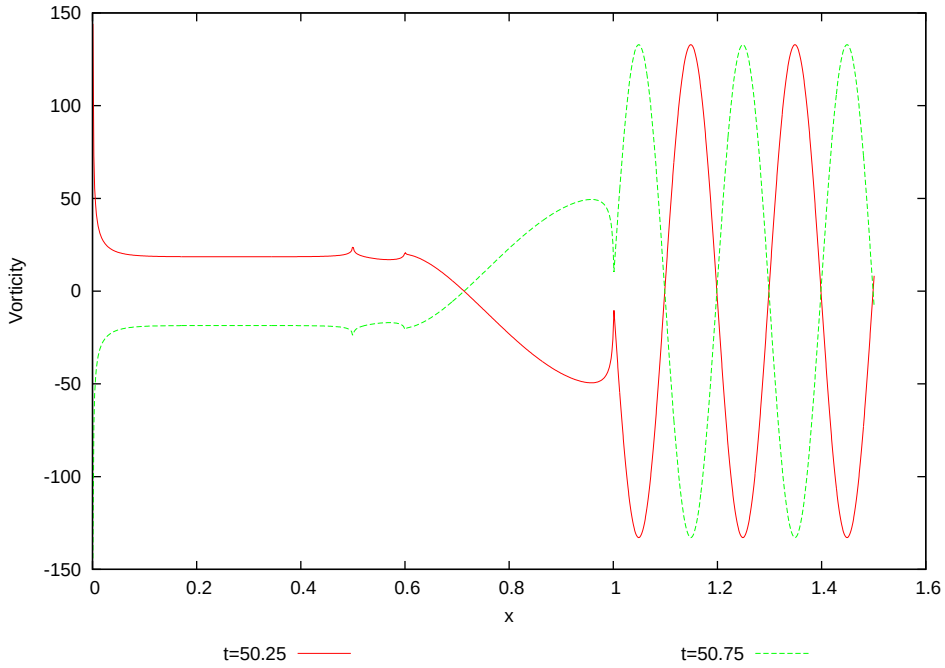

Figure 4.16: Vorticity at $t = 50.25, 50.75$, for $Sr = 5.0$, $\beta = 0.9630$ and $\delta = 5.0$

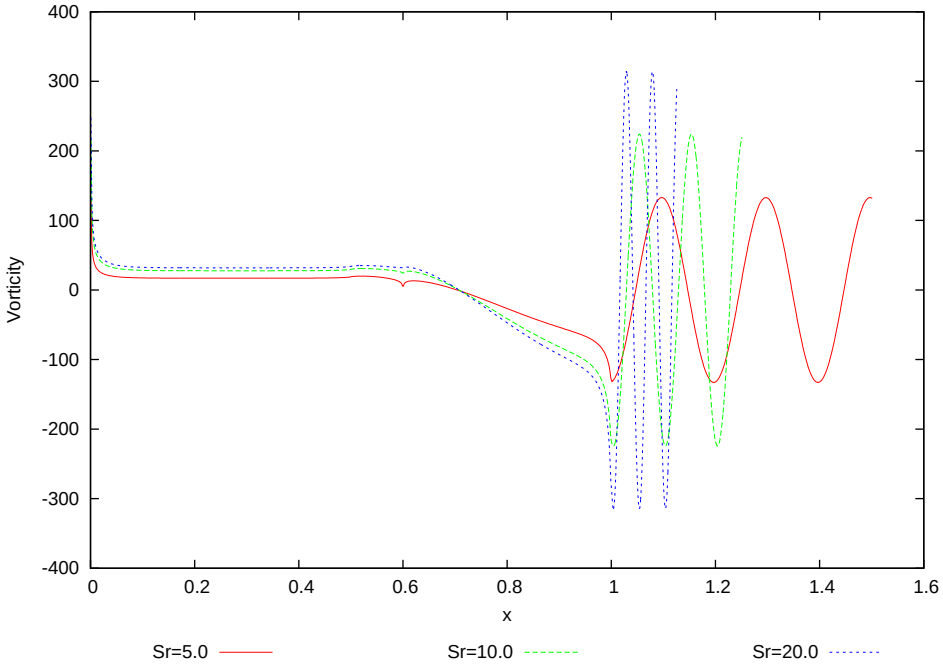

Figure 4.17: Comparison of Vorticity at $t = 50.9975$, for $Sr = (5.0, 10.0, 20.0)$, $\beta = 0.9630$ and $\delta = 5.0$

Table 4.4: Horizontal forces for different Strouhal numbers at $\alpha = 1.2323$, $\beta = 0.9630$ and $\delta = 5.0$

Strouhal Number (Sr)	Horizontal Force (F_p)	Leading Edge Thrust (F_{le})
5.0	-74.188123	-13.019872
10.0	-108.50512	-19.185041
20.0	-119.14272	-20.993670
100.0	-112.02315	-19.432259

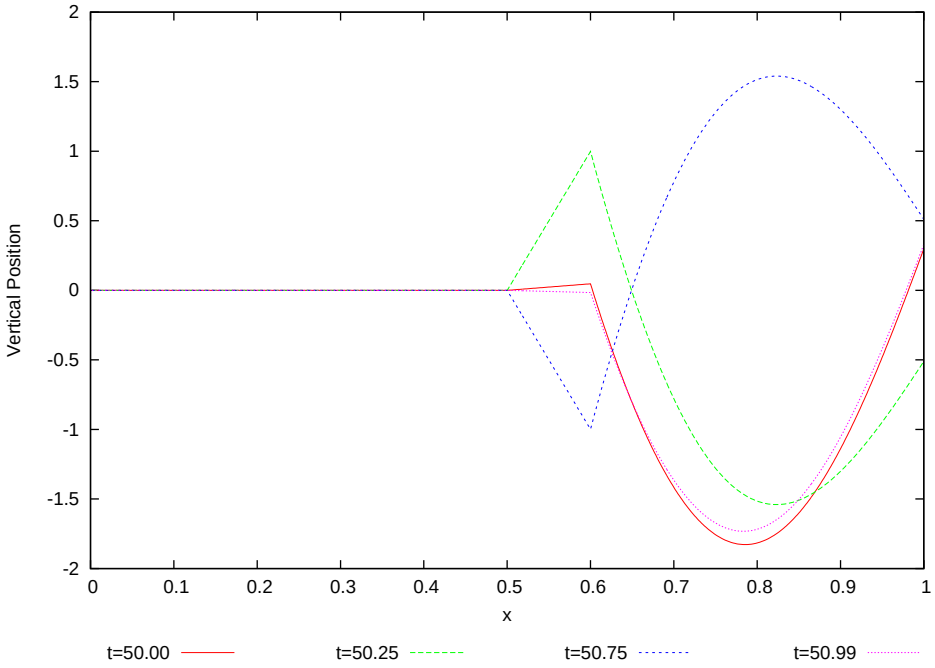

Figure 4.18: Vertical position at $t = (50.0, 50.25, 50.75, 50.9975)$, for $Sr = 5.0$, $\beta = 0.9630$ and $\delta = 10.0$

4.5 Variation of Strouhal number keeping $\beta = 0.9630$ and $\delta = 10.0$

In this section width of channel has been decreased so length to width ratio $\delta = 10.0$. The tensions in the membrane have been kept same as in the previous case. So the dimensionless constants $\alpha = 1.2323$ and $\beta = 0.9630$. Vertical position of the membrane after 50 periods at $t = 50.0$, $t = 50.25$, $t = 50.75$ and $t = 50.9975$ is shown in figure 4.18. In figure 4.19 the vertical positions of membrane at $t = 50.9975$ (when the flap is at near to its mean position) for different Strouhal numbers have been compared. In figure 4.20 the vorticities on the membrane and in the wake at $t = 50.9975$ for different Strouhal numbers have been compared. The vorticity increase monotonically by increasing the Strouhal number. In table 4.5 periodic horizontal force and the leading edge thrust are shown for different Strouhal numbers keeping $\delta = 10.0$ and $\beta = 0.9630$. The table 4.5 clearly shows that we get maximum net horizontal forces when we have the maximum Strouhal number. Therefore at this aspect ratio and tensions in the membrane the net thrust of the double channel membrane pump increases monotonically by increasing the Strouhal number.

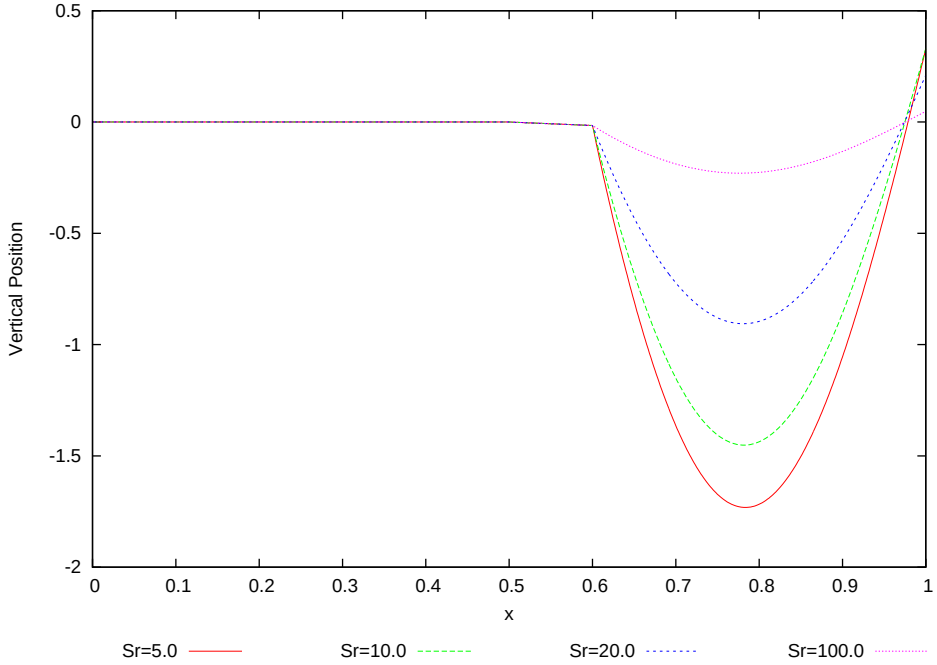

Figure 4.19: Comparison of the vertical position at $t = 50.9975$, for $Sr = (5.0, 10.0, 20.0, 100.0)$, $\beta = 0.9630$ and $\delta = 10.0$

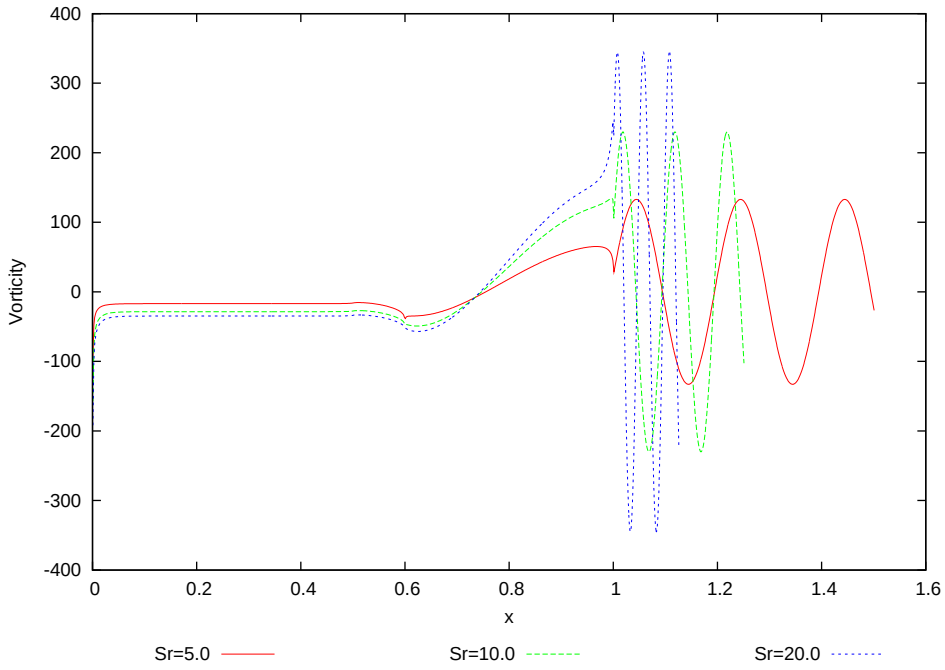

Figure 4.20: Comparison of the vorticity at $t = 50.9975$, for $Sr = (5.0, 10.0, 20.0)$, $\beta = 0.9630$ and $\delta = 10.0$

Table 4.5: Horizontal forces for different Strouhal numbers at $\alpha = 1.2323$, $\beta = 0.9630$ and $\delta = 10.0$

Strouhal Number (Sr)	Horizontal Force (F_p)	Leading Edge Thrust (F_{le})
5.0	-73.937091	-9.2666042
10.0	-120.01114	-14.742523
20.0	-146.97783	-17.964578
100.0	-179.50642	-21.856431

4.6 Variation of Strouhal number keeping $\beta = 0.9630$ and $\delta = 20.0$

In this section width of channel has been further decreased so length to width ratio $\delta = 20.0$. The tensions in the membrane have been kept same as in the previous case. Vertical position of the membrane after 50 periods at $t = 50.0$, $t = 50.25$ and $t = 50.75$ is shown in figure 4.21. In figure 4.22 the vertical positions of membrane at time $t = 50.9975$ for different Strouhal numbers have been compared. In figure 4.23 the vorticities on the membrane and in the wake at $t = 50.9975$ for different Strouhal numbers have been compared. The vorticity increases by increasing the Strouhal number. In table 4.6 periodic horizontal force and the leading edge thrust are shown for different Strouhal numbers keeping $\delta = 20.0$ and $\beta = 0.9630$. The horizontal pressure force increases by increasing the Strouhal number but the increase in the horizontal force is minmal. Thefore we observe at high aspect ratio the net thrust of the double channel membrane pump does not improve by increasing the Strouhal number. Also the leading edge thrust decrease instead of increasing by increasing the Strouhal number due to high aspect ratio.

4.7 Variation of Strouhal number keeping $\beta = 0.0000963$ and $\delta = 5.0$

In this section the tensions of the membrane have been assumed very small. For small tensions in the membrane the dimensionless constant α has been kept same ($\alpha = 1.2323$) where as value of β has been decreased considerably. The width of channel has been kept large so length to width ratio $\delta = 5.0$. Vertical position of the membrane after the 50 periods at time $t = 50.0$

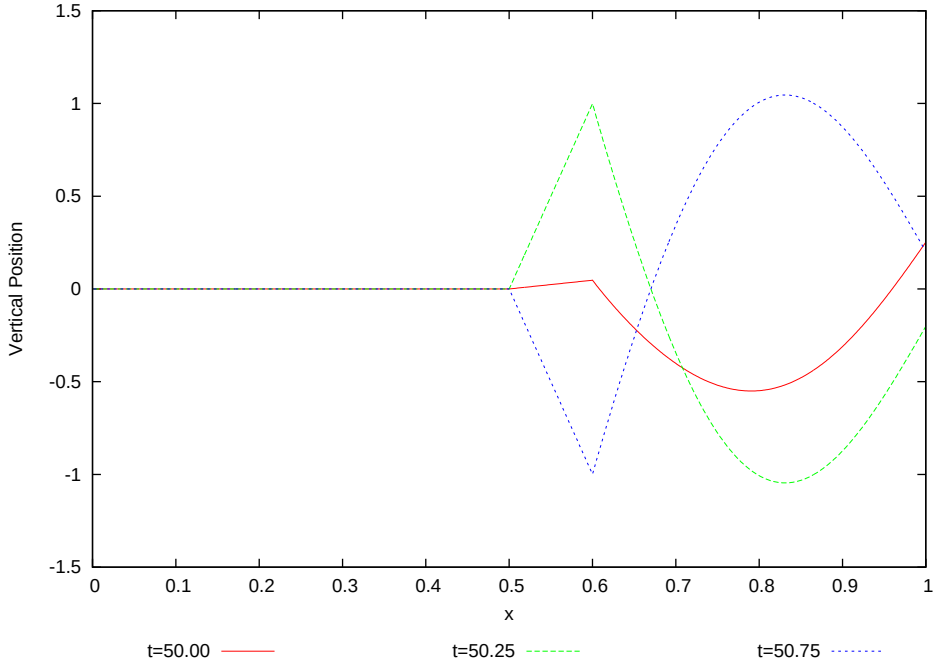

Figure 4.21: Vertical position at $t = (50.0, 50.25, 50.75)$, $Sr = 5.0$, for $\beta = 0.9630$ and $\delta = 20.0$

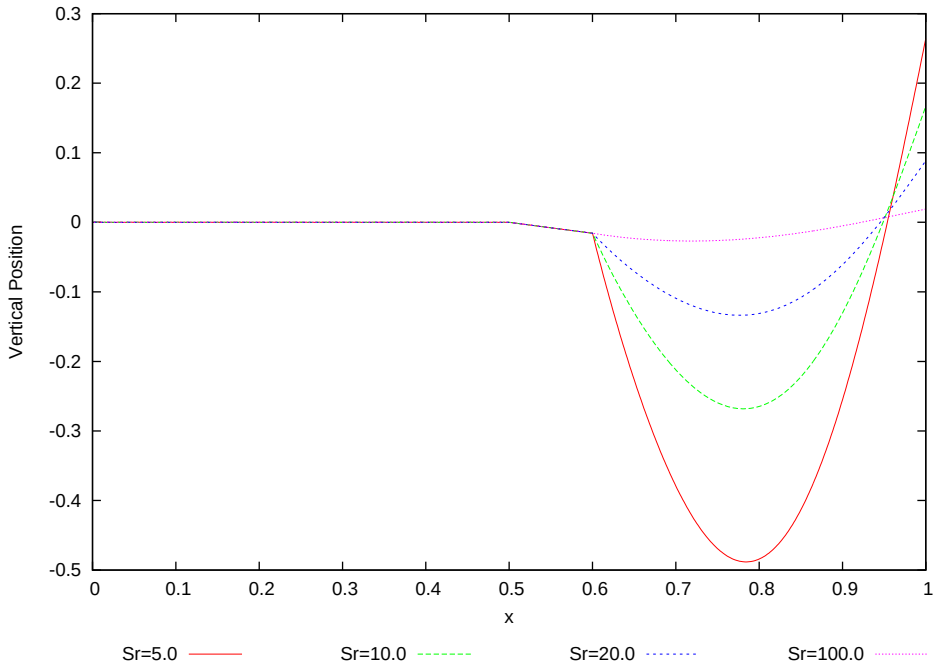

Figure 4.22: Comparison of the vertical position at $t = 50.9975$, for $Sr = (5.0, 10.0, 20.0, 100.0)$, $\beta = 0.9630$ and $\delta = 20.0$

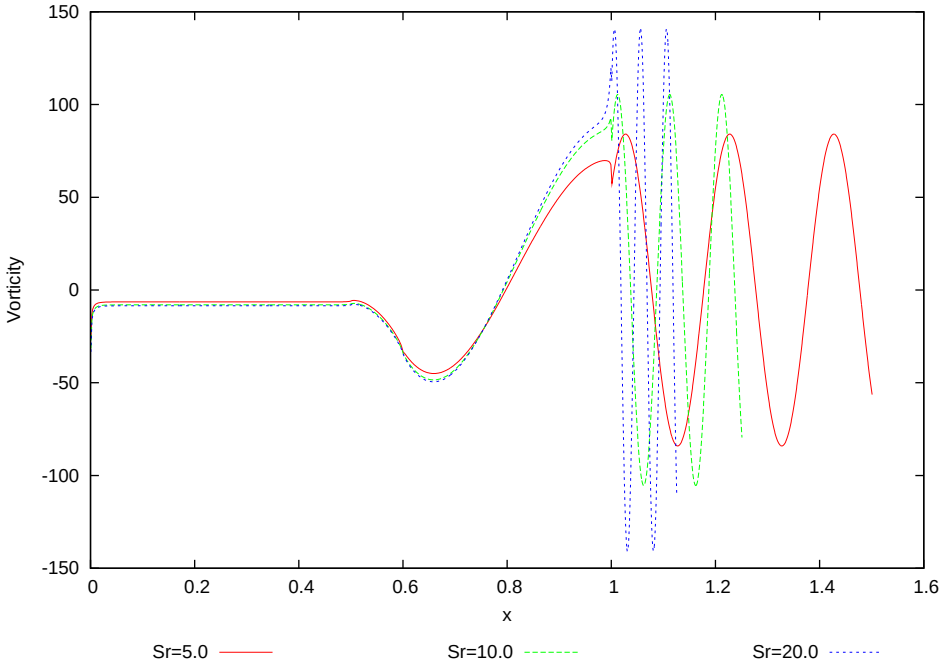

Figure 4.23: Comparison of the vorticity at $t = 50.9975$, for $Sr = (5.0, 10.0, 20.0)$, $\beta = 0.9630$ and $\delta = 20.0$

Table 4.6: Horizontal forces for different Strouhal numbers at $\alpha = 1.2323$, $\beta = 0.9630$ and $\delta = 20.0$

Strouhal Number (Sr)	Horizontal Force (F_p)	Leading Edge Thrust (F_{le})
5.0	-23.294548	-1.3499736
10.0	-24.920043	-1.0050259
20.0	-25.532188	-0.9173310
100.0	-27.093723	-1.0090380

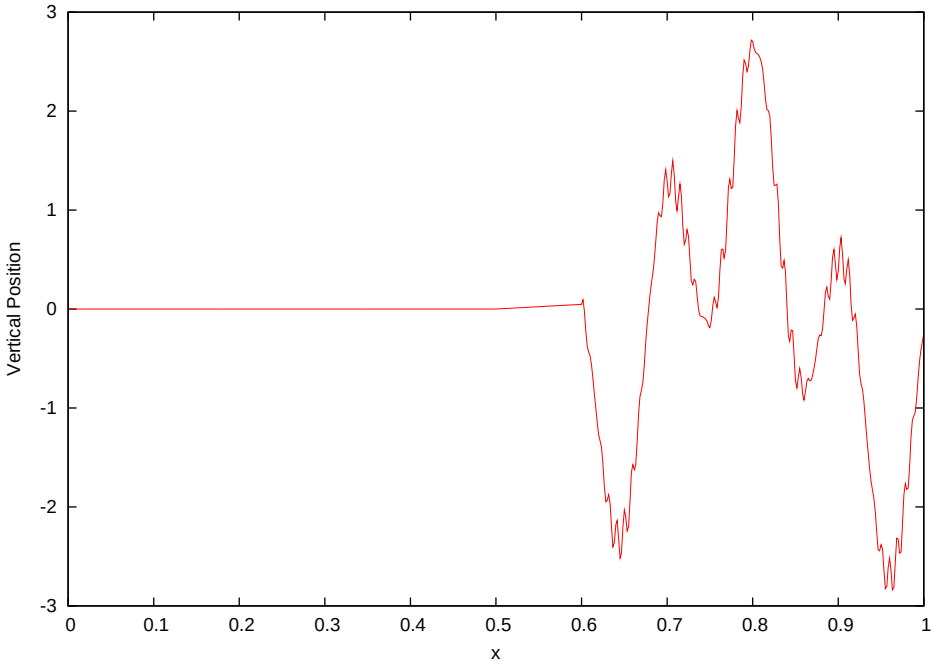

Figure 4.24: Vertical position at $t = 50.0$, for
$Sr = 5.0$, $\beta = 0.0000963$ and $\delta = 5.0$

(flap is at its mean position) for $Sr = 5.0$ is shown in figure 4.24. It is evident from the figure 4.24 that there are a lot of kinks in the membrane. These kinks are due to the small tension in the membrane. The tension in the membrane is very important factor and it should not be less than a certain value to get better results. In figure 4.25 the vertical positions of membrane after 50 periods at $t = 50.0$ (when the flap is at its mean position) for different Strouhal numbers have been plotted. In figure 4.26 Vorticity on the membrane and in the wake after 50 periods for Strouhal number has been shown. The vorticity increases by increasing the Strouhal number. In table 4.7 periodic horizontal force and the leading edge thrust are shown for different Strouhal numbers keeping $\delta = 5.0$ and $\beta = 0.0000963$. The horizontal forces increases by increasing the Strouhal number but there value is very small as compared to cases where we have greater tensions in the membrane.

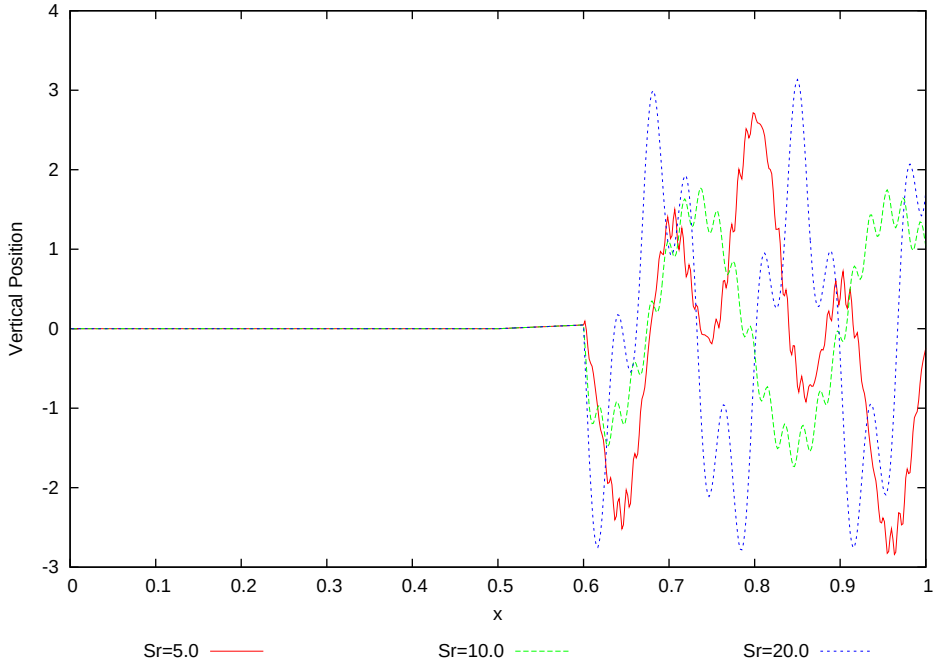

Figure 4.25: Comparison of the vertical position at $t = 50.0$, for $Sr = (5.0, 10.0, 20.0)$, $\beta = 0.0000963$ and $\delta = 5.0$

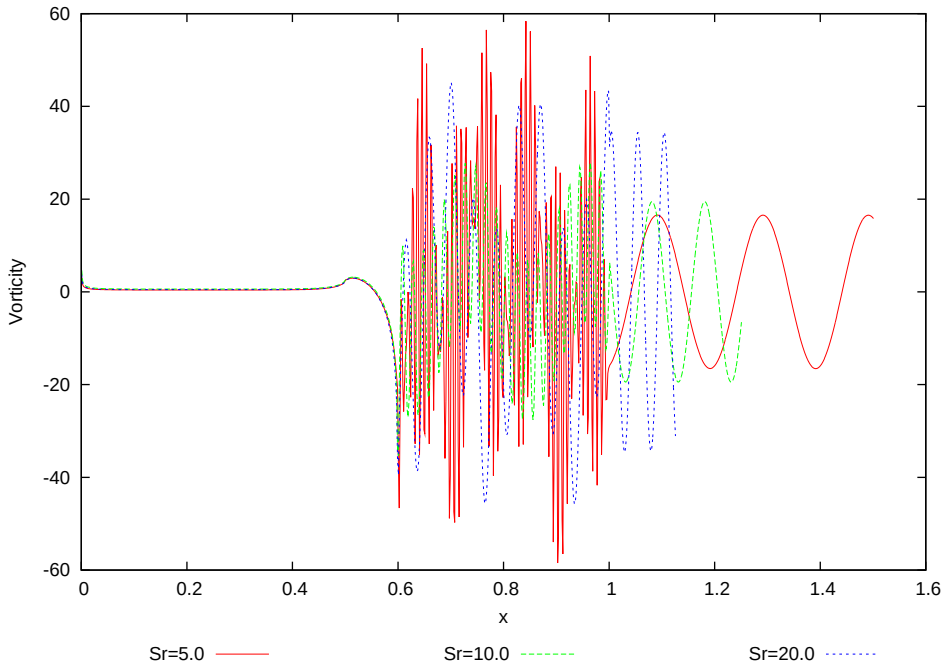

Figure 4.26: Comparison of the vorticity at $t = 50.0$, for $Sr = (5.0, 10.0, 20.0)$, $\beta = 0.0000963$ and $\delta = 5.0$

Table 4.7: Horizontal forces for different Strouhal numbers at $\alpha = 1.2323$, $\beta = 0.0000963$ and $\delta = 5.0$

Strouhal Number (Sr)	Horizontal Force (F_p)	Leading Edge Thrust (F_{le})
5.0	-0.9965749	-0.021663699
10.0	-1.9760069	-0.012321372
20.0	-2.8987964	-0.007592321
100.0	-18.793488	-0.041112337

Table 4.8: Horizontal forces for different Strouhal numbers at $\alpha = 1.2323$, $\beta = 0.0000963$ and $\delta = 10.0$

Strouhal Number (Sr)	Horizontal Force (F_p)	Leading Edge Thrust (F_{le})
5.0	-1.8428088	-0.043311098
10.0	-2.3743485	-0.024824481
20.0	-2.8516584	-0.01409201
100.0	-24.051622	-0.057366079

4.8 Variation of Strouhal number keeping $\beta = 0.0000963$ and $\delta = 10.0$

In this section the tensions of the membrane have been kept same as in the previous case. So the dimensionless constants $\alpha = 1.2323$ and $\beta = 0.0000963$. The width of channel has been decreased so length to width ratio $\delta = 10.0$. Vertical position of the membrane after the 50 periods at $t = 50.0$ (flap is at its mean position) for $Sr = 5.0$ is shown in figure 4.27. In figure 4.28 the vertical positions of membrane after 50 periods at $t = 50.0$ (when the flap is at its mean position) for different Strouhal numbers are plotted. In figure 4.29 the vorticities on the membrane and in the wake after 50 periods at $t = 50.0$ for different Strouhal numbers is shown. In table 4.8 periodic horizontal force and the leading edge thrust are shown for different Strouhal numbers keeping $\delta = 10.0$ and $\beta = 0.0000963$. As in the previous case the net horizontal forces increases by increasing the Strouhal number at this aspect ratio but they have small values due to less tension in the membrane.

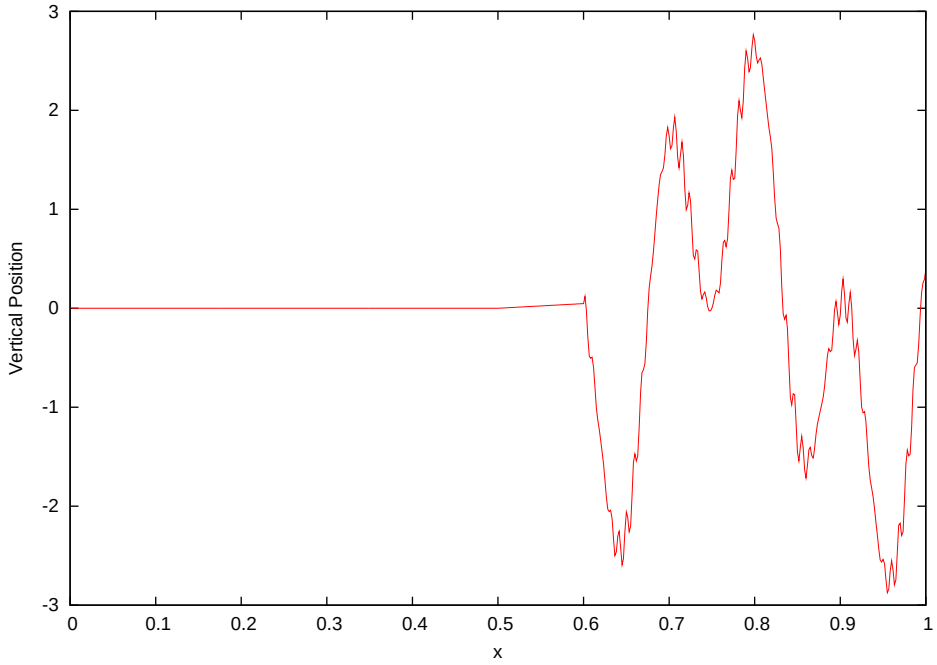

Figure 4.27: Vertical position at $t = 50.0$, for $Sr = 5.0$, $\beta = 0.0000963$ and $\delta = 10.0$

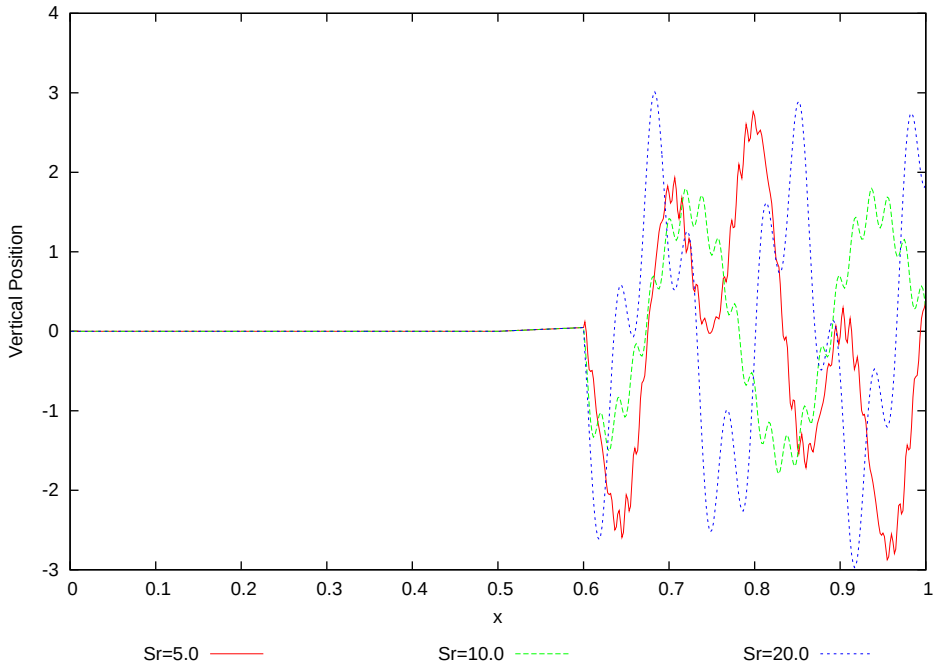

Figure 4.28: Comparison of the vertical position at $t = 50.0$, for $Sr = (5.0, 10.0, 20.0)$, $\beta = 0.0000963$ and $\delta = 10.0$

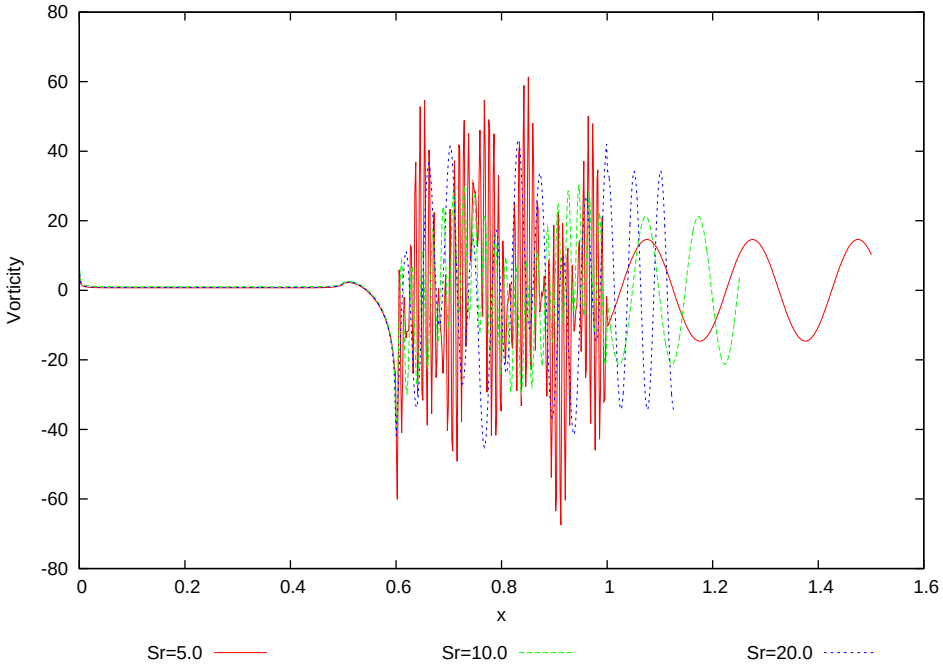

Figure 4.29: Comparison of the vorticity at $t = 50.0$, for $Sr = (5.0, 10.0, 20.0)$, $\beta = 0.0000963$ and $\delta = 10.0$

4.9 Variation of Strouhal number keeping $\beta = 0.0000963$ and $\delta = 20.0$

In this section the tensions of the membrane have been kept same as in the previous case. So the dimensionless constants $\alpha = 1.2323$ and $\beta = 0.0000963$. The width of channel has been further decreased so length to width ratio $\delta = 20.0$. Vertical position of the membrane after the 50 periods at $t = 50.0$ (flap is at its mean position) for $Sr = 5.0$ is shown in figure 4.30. We can see from figure 4.30 that there are kinks in the membrane but these kinks are less as compared to the case where we have low aspect ratio tension in the membrane being the same. In figure 4.31 the vertical positions of membrane at $t = 50.0$ (when the flap is its mean position) for different Strouhal numbers are plotted. In figure 4.32 the vorticities on the membrane and in the wake after 50 periods at $t = 50.0$ for different Strouhal numbers have been compared. In table 4.9 periodic horizontal force and the leading edge thrust are shown for different Strouhal numbers keeping $\delta = 20.0$ and $\beta = 0.0000963$. It is evident from 4.9 that horizontal forces have comparatively less values due to less tension in the membrane. But here due to high aspect ratio we see the net horizontal forces decrease by

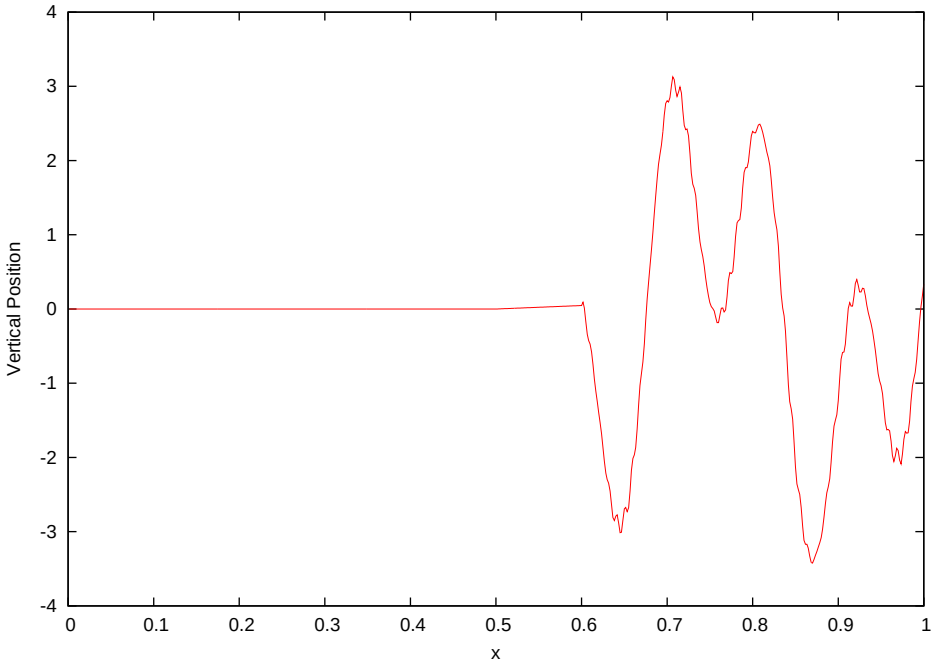

Figure 4.30: Vertical position at $t = 50.0$, for $Sr = 5.0$, $\beta = 0.0000963$ and $\delta = 20.0$

increasing the Strouhal number. Therefore the length to width ratio of a channel is very important to get higher net thrust of the pump. The channel should not be to narrow to get the optimum value of net horizontal forces.

4.10 Net Thrust and Efficiency of the Pump

In this section periodic net thrust values and propulsive efficiency of the pump for different simulations have been compared. The net thrust and propulsive efficiency of the pump depend on the four dimensionless constants used in this work α, β, δ and Sr. In table 4.10 the net thrust and the propulsive efficiency values for different simulations have been shown. In figure 4.33 the net periodic thrust on the membrane as a function of Strouhal number is plotted. The general trend is that the net thrust increases when the Strouhal number is increased. But in some cases we do not get the maximum thrust when the Strouhal number is maximum. For example when β the tension in the string is taken 0.0096 and the channel is wide i,e $\delta = 5.0$ we have maximum thrust at $Sr = 10.0$ instead of $Sr = 100.0$. Also at $\beta = 0.0000963$ for narrow channel ($\delta = 20.0$) the net forces decreases by increasing the Strouhal number. The tensions in the membrane are very important for net thrust.

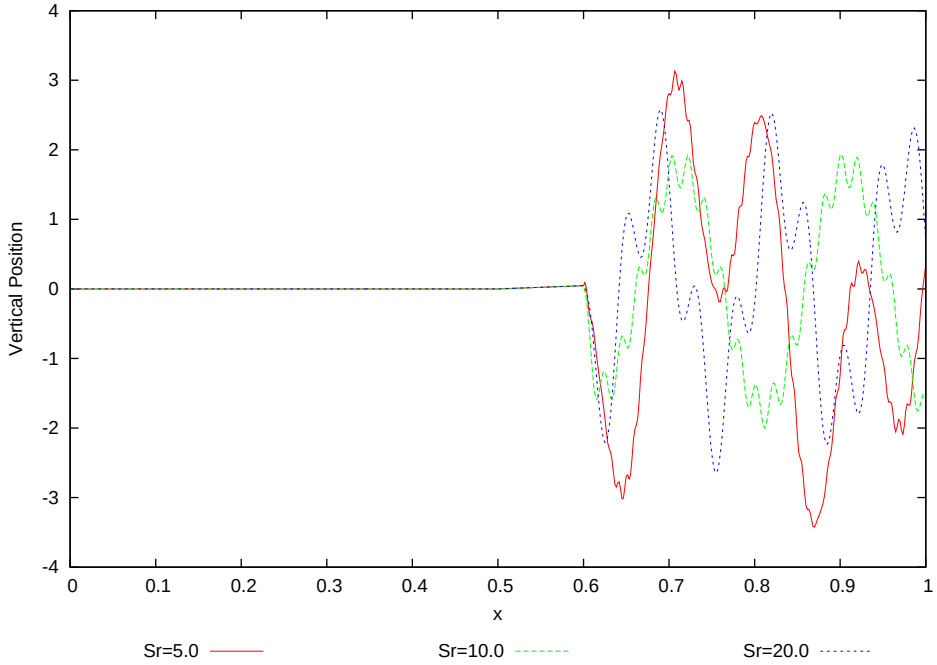

Figure 4.31: Comparison of the vertical position at $t = 50.0$, for $Sr = (5.0, 10.0, 20.0)$, $\beta = 0.0000963$ and $\delta = 20.0$

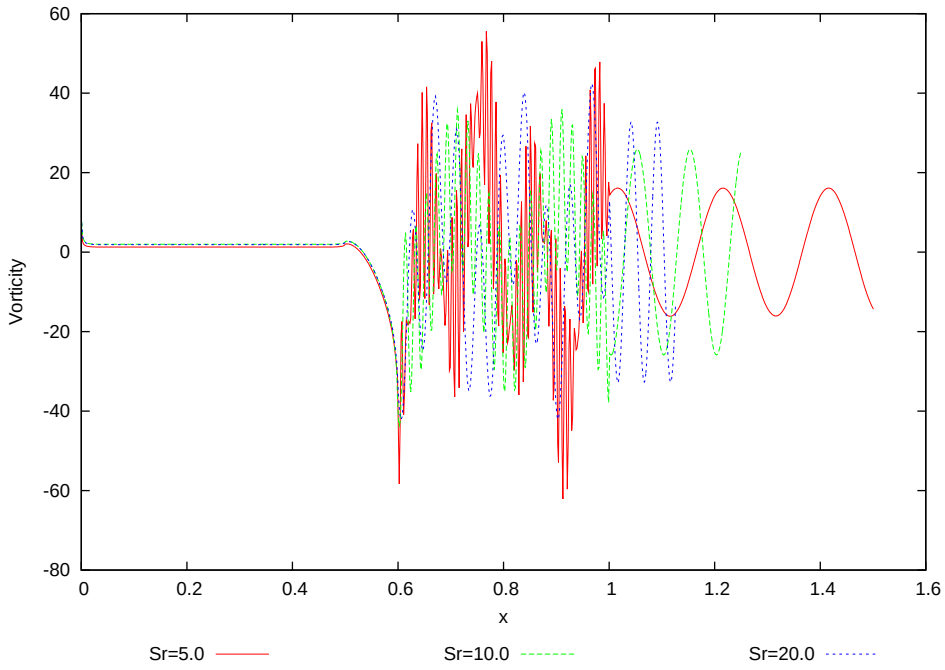

Figure 4.32: Comparison of the vorticity at $t = 50.0$, for $Sr = (5.0, 10.0, 20.0)$, $\beta = 0.0000963$ and $\delta = 20.0$

Table 4.9: Horizontal forces for different Strouhal numbers at $\alpha = 1.2323$, $\beta = 0.0000963$ and $\delta = 20.0$

Strouhal Number (Sr)	Horizontal Force (F_p)	Leading Edge Thrust (F_{le})
5.0	-3.7674449	-0.12161238
10.0	-3.3857728	-0.06940271
20.0	-2.5899370	-0.04710858
100.0	-1.5552597	-0.03501250

By increasing the tensions in the membrane net thrust increases. But it also depends on the aspect ratio. The net thrust increases with increase of aspect ratio but if aspect ratio is too large the net thrust decreases. At $\delta = 10.0$ we have maximum net net thrust keeping other parameters same. In figure 4.34 the propulsive efficiency of the pump as a function of Strouhal number for different simulations is plotted. The efficiency of the pump decreases by increasing the Strouhal number. Also we can see from figure 4.34 the propulsive efficiency is higher when the tension in the membrane is less but for less tension in the membrane the net thrust of the pump is very low. To get the optimum design tension in the membrane should be high. As we have seen earlier the net thrust increases by increasing Strouhal number where as efficiency decreases. Therefore we get optimum design of the double channel membrane pump at $\alpha = 1.2323$, $\beta = 0.9630$, $\delta = 10.0$ and $Sr = 10.0$.

Table 4.10: Periodic net thrust and efficiency of the pump

α	β	δ	Sr	F_p	F_{le}	F	η
1.2323	0.9630	5.0	5.0	-74.188123	-13.019872	-87.207995	0.56
1.2323	0.9630	5.0	10.0	-108.50512	-19.185041	-127.690161	0.49
1.2323	0.9630	5.0	20.0	-119.14272	-20.993670	-140.136390	0.32
1.2323	0.9630	5.0	100.0	-112.02315	-19.432259	-131.455409	0.29
1.2323	0.9630	10.0	5.0	-73.937091	-9.2666042	-83.203732	0.57
1.2323	0.9630	10.0	10.0	-120.01114	-14.742523	-134.753661	0.52
1.2323	0.9630	10.0	20.0	-146.97783	-17.964578	-164.942412	0.38
1.2323	0.9630	10.0	100.0	-179.50642	-21.856431	-201.362850	0.32
1.2323	0.9630	20.0	5.0	-23.294548	-1.3499736	-24.644522	0.58
1.2323	0.9630	20.0	10.0	-24.920043	-1.0050259	-25.925069	0.53
1.2323	0.9630	20.0	20.0	-25.532188	-0.9173310	-26.449519	0.46
1.2323	0.9630	20.0	100.0	-27.093723	-1.0090380	-28.102761	0.13
1.2323	0.00963	5.0	5.0	-1.7982950	-0.0364110	-1.834706	0.69
1.2323	0.00963	5.0	10.0	-6.5248620	-0.2089410	-6.733803	0.58
1.2323	0.00963	5.0	20.0	-3.2276030	-0.1339940	-3.361597	0.70
1.2323	0.00963	5.0	100.0	-2.2890366	-0.09569100	-2.384728	0.11
1.2323	0.00963	10.0	5.0	-2.1374366	-0.07629770	-2.213734	0.72
1.2323	0.00963	10.0	10.0	-5.5628758	-0.07678590	-5.639662	0.59
1.2323	0.00963	10.0	20.0	-18.900380	-0.33572610	-19.236142	0.51
1.2323	0.00963	10.0	100.0	-82.267114	-1.65355220	-83.920666	0.45
1.2323	0.00963	20.0	5.0	-7.8345709	-0.48526679	-8.319838	0.82
1.2323	0.00963	20.0	10.0	-2.9180772	-0.16469291	-3.082770	0.65
1.2323	0.00963	20.0	20.0	-2.4917719	-0.09715820	-2.588930	0.50
1.2323	0.00963	20.0	100.0	-2.2168028	-0.07194497	-2.288748	0.11
1.2323	0.0000963	5.0	5.0	-0.9965749	-0.02166369	-1.018239	0.43
1.2323	0.0000963	5.0	10.0	-1.9760069	-0.01232137	-1.988328	0.74
1.2323	0.0000963	5.0	20.0	-2.8987964	-0.00759232	-2.906389	0.56
1.2323	0.0000963	5.0	100.0	-18.793488	-0.04111233	-18.834600	0.33
1.2323	0.0000963	10.0	5.0	-1.8428088	-0.04331109	-1.886120	0.63
1.2323	0.0000963	10.0	10.0	-2.3743485	-0.02482448	-2.399173	0.71
1.2323	0.0000963	10.0	20.0	-2.8516584	-0.01409201	-2.865750	0.58
1.2323	0.0000963	10.0	100.0	-24.051622	-0.05736607	-24.108988	0.34
1.2323	0.0000963	20.0	5.0	-3.7674449	-0.12161238	-3.889057	0.85
1.2323	0.0000963	20.0	10.0	-3.3857728	-0.06940271	-3.455176	0.73
1.2323	0.0000963	20.0	20.0	-2.5899370	-0.04710858	-2.637046	0.67
1.2323	0.0000963	20.0	100.0	-1.5552597	-0.03501250	-1.590272	0.21

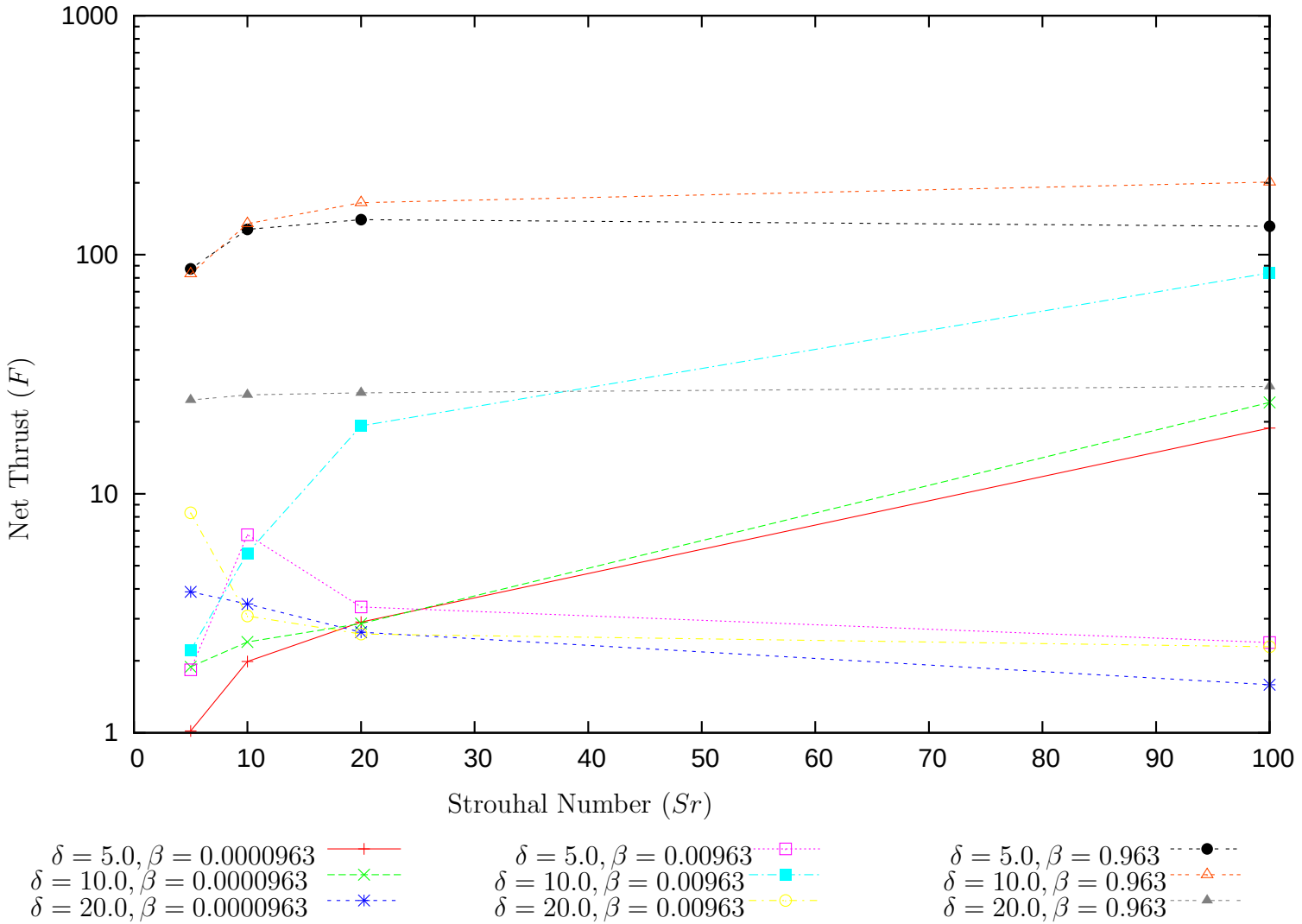

Figure 4.33: Comparison of net periodic thrust

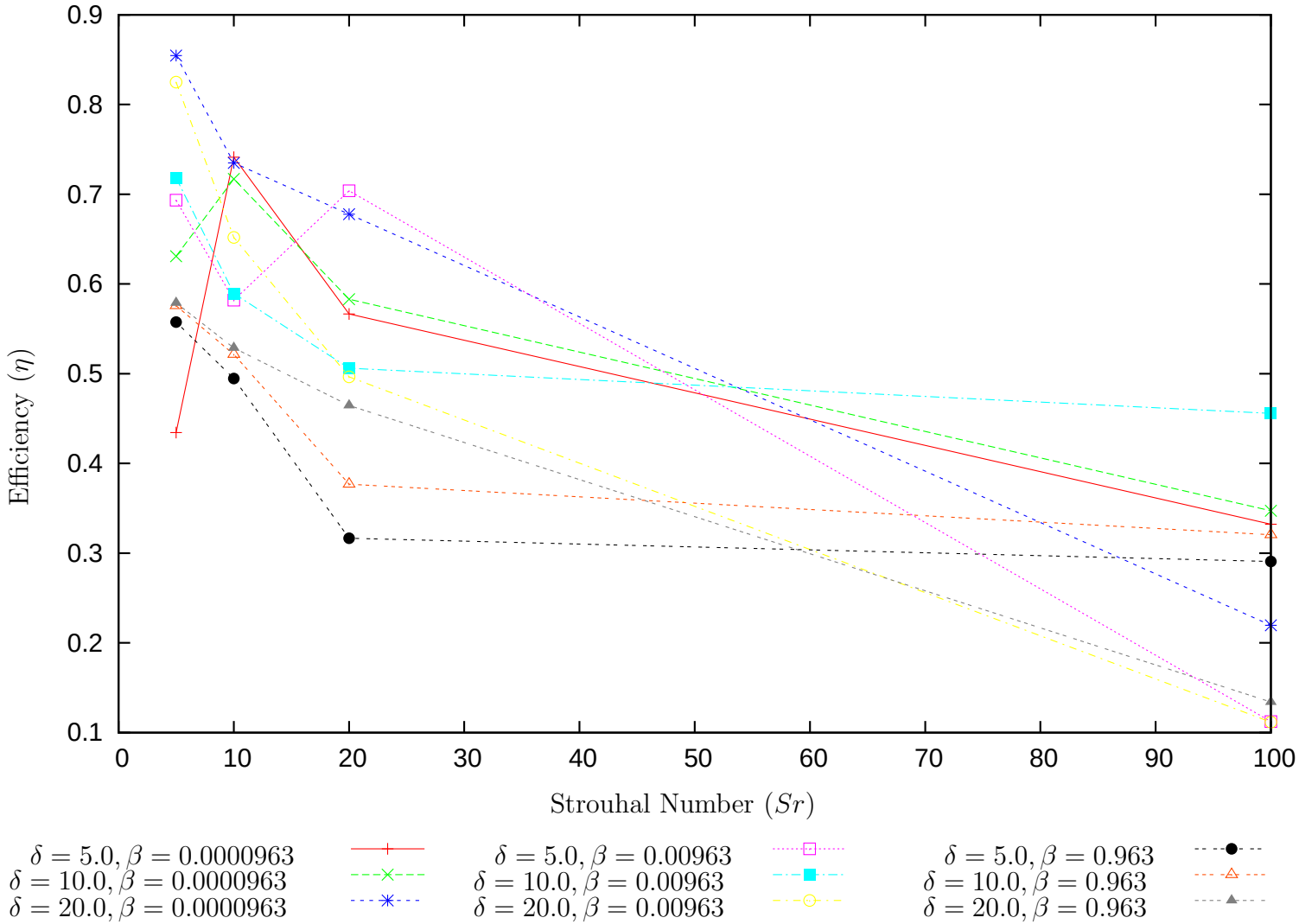

Figure 4.34: Comparison of propulsive efficiency

Chapter 5

Summary

We have presented here a method, which allows the modeling of fluid structure interaction. The method has successfully applied to the investigation of deflections of a thin membrane in unsteady flow. The fluid flow has been assumed two dimensional and high Reynolds number flow. Further it is assumed that flow is incompressible and irrotational. It is clear that pressure difference across the membrane is the primary mechanism for pumping principal. This pressure difference across the membrane has been calculated using unsteady Bernoulli's equation. From this pressure difference we have calculated the horizontal force on the membrane. The leading edge thrust also has been approximated. Then we have calculated the net thrust and propulsive efficiency of the pump. The net thrust of the pump increases with increasing Strouhal number where has propulsive efficiency decreases by increasing the Strouhal number. The tension in the membrane is also very important. By increasing the tension in the membrane we get higher values of net thrust but efficiency drops a little bit. Aspect ratio of the pump is another factor to find the optimum design. The channel should not be too narrow neither it should be too wide. An optimum design has been found for the net thrust and efficiency of the pump.

Bibliography

[1] Betz, A. (1912): Ein Beitrag zur Erklärung des Segelfluges. Zeitschrift für Flugtechnik und Motorluftschiffahrt, 3, pp. 269-272.

[2] Birnbaum, (1924): Schlagflugelpropeller und die kleinen Schwingungen elastisch befestigter Tragflugel, Zeitschrift für Flugtechnik und Motorluftschiffahrt.

[3] Borzi, A. and Propst, G. (2003): Numerical investigation of the Liebau phenomenon, Math. Phys. 54, pp. 1050-1072.

[4] Brezinski, C. and Redivo Zaglia M. (1991): Extrapolation Methods: Theory and Practice, North-Holland. Amsterdam.

[5] Carling, J., Williams, T., Bowtell, G.(1998): Self-propelled Anguilliform swimming: simultaneous solution of the two-dimensional NavierStokes equations and Newton's laws of motion. J. Exp. Biol. 201 pp.3143-3166.

[6] Cebeci, Tuncer (1999): An engineering approch to the calculation of aerodynamic flows, Springer.

[7] Cheng,J.Y., Zhuang, L.X., Tong, B.-G. (1991): Analysis of swimming three-dimensional waving plates. J. Fluid Mech. 232 pp. 341-355.

[8] Daniel, T.L. (1984): Unsteady aspects of aquatic locomotion. Amer. Zool, 24 pp. 121-134.

[9] Daniel, T.L. (1988): Forward flapping flight from flexible fins. Can. J. Zool, 6 pp. 630-638.

[10] De Hart, J., Peters, G.W.M., Schreurs, P.J.G., Baaijens, F.P.T. (2000): A two-dimensional fluid-structure interaction model of the aortic value, J. Biomech., 33(9) pp. 1079- 1088.

[11] De Hart, J., Peters, G.W.M., Schreurs, P.J.G., Baaijens, F.P.T. (2003): A three-dimensional computational analysis of fluid-structure interaction in the aortic valve. J. Biomech., 36(1) pp. 103-112.

[12] Drucker, E.G., Lauder, G.V. (2000): A hydrodynamic analysis of fish swimming speed: Wake structure and locomotor force in slow and fast labriform swimmers. J. Exp. Biol. 203 pp. 2379-2393.

[13] Drucker, E.G., Lauder, G.V. (2002): Wake dynamics and locomotor function in fishes: Interpreting evolutionary patterns in pectoral fin design Integr. Comp. Biol. 42:-000.

[14] Farnell, D.J.J, David, T., Barton, D.C. (2004) Coupled states of flapping flags. J. Fluids Struct. 19 pp. 29-36.

[15] Farnell, D.J.J., David, T., Callaghan, F., Barton, D.C. (2004): Flexible membranes in flowing fluids. FIV2004, 8th International Conference on Flow-Induced Vibrations, Ecole Polytechnique, Paris.

[16] Fenlon, A.J., David, T. (2001): Numerical models for the simulation of flexible leaflet heart valves. Part 1. Computational methods. Comput. Methods Biomech. Biomed. Eng. 4 pp. 323-339.

[17] Fenlon, A.J., David, T. (2001): Numerical models for the simulation of flexible leaflet heart valves. Part 2. Valve studies. Comput. Methods Biomech. Biomed. Eng. 4 pp. 449-462.

[18] Freymuth, P. (1988): Propulsive vortical signature of plunging and pitching airfoils, AIAA J 26, pp. 881-883.

[19] Garrick, I.E.: Propulsion of a flapping and oscillating airfoil. NACA TR 567.

[20] Glück, M., Breuer M., Durst, F., Halfmann, A., Rank, E. (2001): Computation of fluid structure interaction on lightweight structures. Journal of Wind Engineering and Industrial Aerodynamics. 89 pp. 1351-1368.

[21] Gray, J. (1933): Studies in animal locomotion. J. Exp. Biol. 10 PP. 88-104.

[22] Gray, J. (1955): The movement of sea-urchin spermatozoa. J. Exp. Biol. 32 pp. 775-801.

[23] Gray, J., Hancock, G.J. (1955): The propulsion of sea-urchin spermatozoa. J. Exp. Biol. 32 pp. 801-814.

[24] Horsten J. B. A. M. (1990): On the analysis of moving heart valves. PhD thesis, TU Eindhoven, The Netherlands.

[25] Huber, G. (2000): Swimming in Flatsea. Nature. 408 pp. 777-778.

[26] John Moores (2003): Potential flow 2-dimensional vortex panel model: Applications to wingmills, Master's thesis. University of Toronto. Faculty of Applied Science and Engineering.

[27] Jones, K. D., Dohring, C. M., and Platzer, M. F. (1998): Experimental and computational inversitigation of the Knoller-Betz effect, AIAA J., Vol. 36, pp. 1240-1246.

[28] Jung, E., Peskin, C. (2001): 2-D simulations of valveless pumping using immersed boundary methods. SIAM J Sci Comput 23(1) pp. 19-45.

[29] Katz J., Plotkin A. (2001): Low-Speed Aerodynamics, Second Edition.

[30] Katzmayr, R.(1922): Effect of periodic changes of angle of attack on behavior of airfoils, NACA CR TM 147.

[31] Knoller, R.(1909): Die Gesetze des Luftwiderstandes. Flug und Motoretechnik, Vol. 3, pp. 1-7.

[32] Koochesfahani, M.M.(1989): Vortical patterns in the wake of an oscillating airfoil, AIAA J 27, pp. 1200-1205.

[33] Lai, J. C. S. and Platzer, M. F.(1999): Jet characteristics of a plunging airfoil, AIAA J, Vol. 37, pp. 1529-1537.

[34] Lewin, G. C. and Haj-Harairi, H. (2003): Modelling thrust generation of a two-dimensional heaving airfoil in a viscous flow," J. Fluid Mech., Vol. 492, pp. 339-362.

[35] Lian, Y., Shyy, W. (2003): Three-dimensional fluid- structure interactions of a membrane wing for micro air vehicle applications. Proceedings of the 44th AIAA/ASME/ASCH/AHS/ASC Structures, Structural Dynamics and Materials Conference, 7-10 April 2003, Norfolk, VA, U.S.A., AIAA 1726.

[36] Liebau, G. (1954): Über ein ventilloses pumpprinzip. Naturwissenschaften 41,327

[37] Lighthill M. J. (1960): Note on the swimming of slender fish. Journal of Fluid Mechanics, 9 pp. 305-317.

[38] Lighthill, M. J. (1970): Aquatic animal propulsion of high hydrodynamical effciency. Journal of Fluid Mechanics, 44 pp. 265-301.

[39] Liu, H., Wassersug, R., Kawachi, K. (1996): A computational fluid dynamic study of tadpole swimming. J. Exp. Biol. 199 pp. 1245-1260.

[40] Liu, H., Kawachi, K. (1999): A numerical study of undulatory swimming. J. Comput. Phys. 155, pp. 223-247.

[41] Liu, H. (2002): Computational biological fluid dynamics: Digitizing and visualizing animal swimming and flying. Integr. Comp. Biol. 42.

[42] Liu, H., and Kato, N. (2003): A numerical analysis of unsteady hydrodynamics of a mechanical pectoral fin. J. Fluids Eng.

[43] Long, J.H., Adcock, B., Root, R.G. (2002): Force transmission via axial tendons in undulating mechanical structure: a dynamic analysis. Comput. Biochem. Physiol. A. 133 pp. 911-929.

[44] McCormick,Barnes W. (1995): Aerodynamics, aeronautics, and flight mechanics, John Wiley and Sons, New York.

[45] Mestreau, E., Lohner, R. (1996): Airbag simulation using fluid structure coupling., Proceedings of the 34th Aerospace Sciences Meeting and Exhibit, 15-18 January 1996, Reno, NV, U.S.A., AIAA-96-0798.

[46] Neef, M. F. and Hummel, D. (2000): Euler solutions for a finite-span flapping wing, Tech. rep., June 2000, Conference on fixed, flapping and rotary wing vehicles at very low Reynolds numbers, Univesity of Norte Dame,INDINA.

[47] Ober, S. (1925): Note on the Katzmayr effect on airfoil drag. NACA TR TN 214.

[48] Olsson, A., Stemme, G. and Stemme, E. (1995): A valve-less planar fluid pump with two pump chambers Sensors Actuators A 46-47, pp. 549-556.

[49] Olsson, A., Enoksson, P., Stemme, G. and Stemme, E. (1996): A valveless planar pump isotropically etched in silicon J.Micrmech. Micrrng., 6, pp. 87-91.

[50] Ottesen, J. (2003): Valveless pumping in a uid- lled closed elastic tubesystem: one-dimensional theory with experimental validation. J Math Biol. 46(4) pp. 309-332.

[51] Parkus, H. (1966): Mechanik der festen körper, Springer.

[52] Rinderknecht, D., Hickerson, A.I. and Gharib, M. (2005): A valveless micro impedance pump driven by electromagnetic actuation, J. Micromech. Microeng. 15, pp. 861-866.

[53] Rozhdestvensky, K. V. and Ryzhov, V. A. (2003): Aerohydrodynamics of flapping-wing propulsors, Progress in Aerospace Science, Vol. 39, pp. 585-633.

[54] Schneider, W. (2005): Lift, thrust and heat due to mixed convection flow past a horizontal plate of finite length, J.Fluid Mech. vol. 529 pp. 51-69.

[55] Schoop, H., Bessert, N. (2001): Instationary aeroelastic computation of yacht sails. International Journal for Numerical Methods in Engineering. 52 pp. 787-803.

[56] Shyy, W., Francois, M., Udaykumar, H.S., N dri, N., Tran-Son-Tay R. (2001): Moving boundaries in micro-scale biofluid dynamics. Applied Mechanics Reviews 54 pp. 405-453.

[57] Simon, J. Hill. (1998): Large Amplitude Fish Swimming. PhD thesis, University of Leeds, Department of Applied Mathematics.

[58] Stemme, E. and Stemme, G. (1993): A valve-less diffuser/nozzle based fluid pump Sensors Actuators A 39, pp. 159-167.

[59] Stemme, E. and Stemme, G. (1993): Valve-less fluid pump Swedish Patent Application, 9, 300, pp. 604-607.

[60] Taylor, G.I. (1952): Analysis of the swimming of long and narrow animals. Proc. R. Soc. A. 214, pp. 158-183.

[61] Tezduyar, T., Osawa, Y. (2001): Fluid structure interactions of a parachute crossing the far wake of an aircraft. Computer Methods in Applied Mechanics and Engineering. 191 pp.717-726.

[62] Theodorsen, T.: General theory of aerodynamic instability and the mechanism of flutter. NACA TR 496.

[63] Thomann, H. (1978): A simple pumping mechanism in a valveless tube. Z Angew Math Phys 29 pp. 169-177.

[64] Triantafyllou, M. S., Triantafyllou, G. S., and Yue, D. K. P.(2000): Hydrodynamics of Fish Swimming, Ann. Rev. Fluid Mech., 32, pp. 33-53.

[65] Triantafyllou, M.S., A. H. Techet, and F.S. Hover,(2004): Review of Experimental Work in Biomimetic Foils, IEEE Journal of Oceanic Engineering, v. 29(3), pp. 585-594.

[66] Triantafyllou, M. S., F.S. Hover, A. H. Techet and D. K. P. Yue, (2005): Review of Hydrodynamic Scaling Laws in Aquatic Locomotion and Fish-like Swimming, Appl. Mech. Review, vol. 58.

[67] Tuncer, I. H. and Platzer, M. F. (2000): Computational study of flapping airfoil aerodynamics, J. of Aircraft, Vol. 37, pp. 514-520.

[68] van Loon, R., Anderson, P.D., van de Vosse, F.N. (2006): A fluid-structure interaction method with solid-rigid contact for heart valve dynamics., Journal of Computational Physics. 217 pp. 806-823. DOI: 10.1016/j.jcp.2006.01.032.

[69] Webb, P. W. (1982): Locomotor patterns in the evolution of actinopterygian fishes. Amer. Zool. 22 pp. 329-342.

[70] Webb, P. W. (1984): Body form, locomotion and foraging in aquatic vertebrates. Amer. Zool. 24 pp. 107-120.

[71] Webb, P. W. (1993): Swimming. In D. H. Evans (ed.), The physiology of fishes, pp. 47-73. CRC Press, Boca Raton.

[72] Wen, C.Y., Cheng, C.H., Jian, C.N., Nguyen, T.A., Hsu, C.Y. and Su,Y.R.(2006): A valveless micro impedence pump driven by PZT actuation, Materials Science Forum 505-507, pp. 127-132. bibitemWu Wu, T.Y.T. (1960): Swimming of a waving plate, Journal of Fluid Mechanics, 10 pp. 321-544.

[73] Wu, T.Y.T. (1971): Hydrodynamics of swimming propulsion, Part 2. Some optimum shape problems, Journal of Fluid Mechanics, 46 pp. 521-544.

[74] Wu, T.Y.T. (1971): Hydrodynamics of swimming propulsion. Part 1. Swimming of a two-dimensional flexible plate at variable speeds in an inviscid fluid. Journal of Fluid Mechanics, 46 pp. 337-355.

[75] Yang S., Lua, S., Liu, F. (2005): Computation of the flows over flapping airfoil by Euler equations,AIAA 43rd Aerospace Science Meeting, Reno, NV, Jan. 10-13,2005.

[76] Young, J. and Lai, J. C. S. (2004): Oscillation frequency and amplitude effects on the wake of a plunging airfoil, AIAA J. Vol. 42, pp. 2042-2052.

[77] Zackl W., Neth H., Steinrück H. (2006): An experimental investigation of a double channel membrane pump.